Article

# Redox-Responsive Halogen Bonding as a Highly Selective Interaction for Electrochemical Separations

Nayeong Kim, Vijaya S. Jeyaraj, Johannes Elbert, Sung Jin Seo, Alexander V. Mironenko, and Xiao Su*

Read Online

ACCESS | Metrics & More | Article Recommendations | Supporting Information

**ABSTRACT:** Leveraging specific noncovalent interactions can broaden the mechanims for selective electrochemical separations beyond solely electrostatic interactions. Here, we explore redox-responsive halogen bonding (XB) for selective electrosorption in nonaqueous media, by taking advantage of directional interactions of XB alongisde a cooperative and synergistic ferrocene redox-center. We designed and evaluated a new redox-active XB donor polymer, poly(5-iodo-4-ferrocenyl-1-(4-vinylbenzyl)-1*H*-1,2,3-triazole) (P(FcTS-I)), for the electrochemically switchable binding and release of target organic and inorganic ions at a heterogeneous interface. Under applied potential, the oxidized ferrocene amplifies the halogen binding site, leading to significantly enhanced uptake and selectivity towards key inorganic and organic species, including chloride, bisulfate, and benzenesulfonate, compared to the open-circuit potential or the hydrogen bonding donor analog. Density functional theory calculations, as well as spectroscopic analysis, offer mechanistic insight into the degree of amplification of $\sigma$-holes at a molecular level, with selectivity modulated by charge transfer and dispersion interactions. Our work highlights the potential of XB in selective electrosorption by uniquely leveraging noncovalent interactions for redox-mediated electrochemical separations.

**KEYWORDS:** *electrochemical separations, ion selectivity, electrosorption, redox-polymers, halogen bonding*
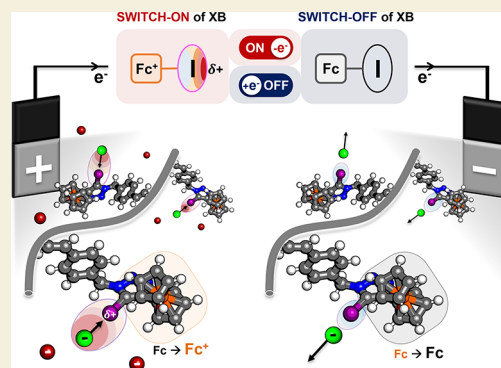
## 1. INTRODUCTION

The design of molecularly selective interactions with strong binding and reversibility is of paramount importance for electrochemically mediated separations in a heterogeneous platform,[1−5] particularly for the sustainable recovery of value-added compounds in nonaqueous media.[6−8] Redox-active platforms have been powerful for the selective recovery of value-added species;[5,9−11] however, their applications have primarily been restricted to ion sorption applications in the aqueous phase, where selective electrosorption has mostly relied on electrostatic interactions between the redox-active motif and ions.[5,12−16] With the growing industries of pharmaceutical or chemical synthesis,[4,17,18] there is an increasing need for the exploration, development, and implementation of tunable intermolecular interactions to expand the scope of selective electrochemical separation to nonaqueous media. Here, we design a redox-responsive halogen bonding polymer with a robust and selective noncovalent interaction for electrochemical separations in nonaqueous media. Our study demonstrates the use of halogen bonding for achieving selective electrosorption and release of target species at a heterogeneous interface via the electrochemical amplification of its intermolecular interaction with a cooperative, synergistic redox center.

Halogen bonding (XB) has emerged as a versatile non-covalent interaction for a wide range of anions, especially halide

molecules.[19−23] XB offers stronger noncovalent interactions toward Lewis bases than hydrogen bonding (HB) in organic media, owing to the highly polarizable nature of the halogen bound on the carbon (e.g., carbon-bound iodine).[20] Thus, the importance of the XB can be found in numerous applications such as the self-assembly of crystals,[24] sensors for both inorganic and organic species,[21,22,25−31] catalysis,[32−34] enantiomer separations,[35] and drug delivery.[22,36,37] Halogen bonding molecules have been deployed in various structural forms, such as small molecules,[38] crystals,[24,39] oligomers,[40] and polymeric structures[41−44] in both homogeneous[45] or heterogeneous platforms as thin films[38,46−48] or coatings on substrates.[31] In addition, XB has been a key interaction in biological systems, such as between the thyroid and its enzyme (iodothyronine deiodinases) to control protein synthesis and bone maturation.[28] The design of redox-responsive motifs with XB donors has been previously explored as an electrochemically switchable sensor by incorporating redox-active units such as ferrocene and

tetrathiafulvalene as electron-withdrawing groups to modulate the strength of the halogen bonding.[21,25] Upon oxidation of the redox-active moiety, it withdraws electron density from the halogen atom, thus forming a lower electron density region, known as $\sigma$-hole. Consequently, the $\sigma$-hole on the halide atom interacts noncovalently with the Lewis base, resulting in robust molecular recognition of the anions, rather than breaking the C—X bond or oxidizing into halogen atoms.

Despite its promising switchability and directional selectivity for ion binding, halogen bonding has not yet been explored for electrochemically mediated separations. Redox-mediated anion recognition studies have mainly focused on homogeneous sensing systems, where both the target species and redox-active molecules are dissolved in organic media.[25−27] However, for electrosorption, a heterogeneous platform is necessary to easily separate the adsorbed target species and XB donor molecules from the initial solution. Although redox-responsive self-assembled monolayers (SAMs) have been extensively studied for surface-confined sensors with their enhanced sensing recognition and faster response,[38,48−51] their limited loading capacity of XB donors makes them challenging to implement in electrosorption for the uptake of bulk target species in solution. Therefore, a tailored molecular architecture design is essential to integrating current state-of-the-art redox-responsive halogen bonding donors into selective electrosorption.

Here, we design and synthesize a new macromolecular platform for leveraging electrochemically responsive XB as a selective interaction for the separation of charged species in organic media (Scheme 1). In this work, we synthesize a halogen

**Scheme 1. Illustration of P(FcTS-I) Electrochemical Responses during the Electrosorption, where the Oxidation of Ferrocene Amplifies a Sigma Hole for the Selective Adsorption and during the Desorption, and where the Reduction of Ferrocene Switches off the Halogen Bonding and Release the Adsorbed Anions**
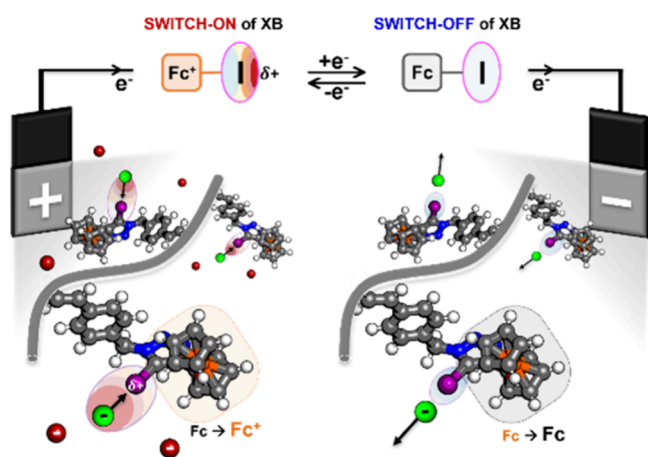


bonding donor metallopolymer, poly(5-iodo-4-ferrocenyl-1-(4-vinylbenzyl)-1*H*-1,2,3-triazole) (P(FcTS-I)), to translate the electrochemically responsive supramolecular recognition onto heterogeneous selective electrosorption. The oxidation of ferrocene in P(FcTS-I) amplifies the partial positive site ($\sigma$-hole) on the iodine atom to form a noncovalent bond with anions. Conversely, the bound species are released upon reduction of the ferrocene moiety. We demonstrate the redox-switchable halogen bonding for electrosorption and anion recognition of a series of halides, oxyanions, and even organic

molecules, highlighting the enhanced selectivity and reversibility of P(FcTS-I) in the heterogeneous platform. To provide evidence of molecular interaction between the $\sigma$-hole and target species, NMR and Raman spectroscopy measurements are carried out in reduced and oxidized states of the redox-active motif. In addition, density functional theory (DFT) calculations offer insights into the molecular-level $\sigma$-hole amplification and highlight the significance of directional intermolecular interactions in promoting the selective binding of XB donor molecules. Overall, the cooperative molecular design of the redox center with the XB donor enables nonaqueous electrosorption through the highly directional noncovalent interaction, offering a unique strategy to control the binding selectivity and reversibility toward electrochemical separations.

## 2. RESULTS AND DISCUSSION

### 2.1. Synthesis of P(FcTS-I) and Its Heterogeneous Electrode Design

A ferrocene-containing halogen bonding donor molecule, 5-iodo-4-ferrocenyl-1-(4-vinylbenzyl)-1*H*-1,2,3-triazole (FcTS-I), was prepared by Cu(I)-catalyzed azide−alkyne cycloaddition (CuAAC) (Figure 1a; see SI 2 for detailed information about synthesis). FcTS-I contains the redox-active ferrocene motif, which serves as a switchable electron-withdrawing group conjugated to 1,2,3-triazoles to facilitate the electron relocation between redox-active ferrocene and the halogen atom (iodine). Since the modulation of XB strength relies heavily on the presence of a conjugated $\pi$ system between the redox moiety and XB, for either amplifying or decreasing the sigma hole,[25,26,45] we demonstrated XB electrosorption with ferrocene moiety as a redox-active group. Ferrocene exhibits notable physical and electrochemical stability, along with low $E_{1/2}$ potential (∼0.15−0.25 V Ag/Ag+),[11,52] offering significant advantages for incorporating it as a redox moiety in our XB molecule. From a synthesis perspective, a wide range of commercially available ferrocene-based building blocks makes it more convenient to synthesize ferrocene molecules with various conjugates.[11] Among halogen atoms, iodine can promote a strong electron-depleting region ($\sigma$-hole) on the elongation of the covalent bond (C−I) due to its high polarizability.[19,36] In addition, our unique halogen bonding donor molecule features a polymerizable styrene moiety. The monomer was polymerized by free-radical polymerization to prepare an organometallic polymer that can be immobilized onto a heterogeneous electrode. A hydrogen bonding donor monomer, 4-ferrocenyl-1-(4-vinylbenzyl)-1*H*-1,2,3-triazole (FcTS), and its polymer were also synthesized as control molecules using similar synthesis methods as FcTS-I (Figure 1b).

Along with $^1$H NMR, $^{13}$C NMR and sets of 2D NMR enabled identifying the structure of FcTS-I and FcTS molecules with corresponding hydrogen and carbon peaks (Figures S2.4−2.13). For FcTS, an extra singlet peak at 8.32 ppm depicted the HB donor site on C8 (Figure 1c and Figure S2.9). Due to the presence of iodine, C8 for FcTS-I was more electron shielded by a heavy atom effect,[53] resulting in the upfield shift from 122.00 (C8 peak for FcTS) to 79.13 ppm (Figure 1d and Figure S2.5 and S2.10). Additional monomer and polymer characterizations, such as mass spectrometry, elemental analysis, Fourier transform infrared spectroscopy, thermogravimetric analysis, X-ray photoelectron spectroscopy, and gel permeation chromatography, can be found in SI 2.
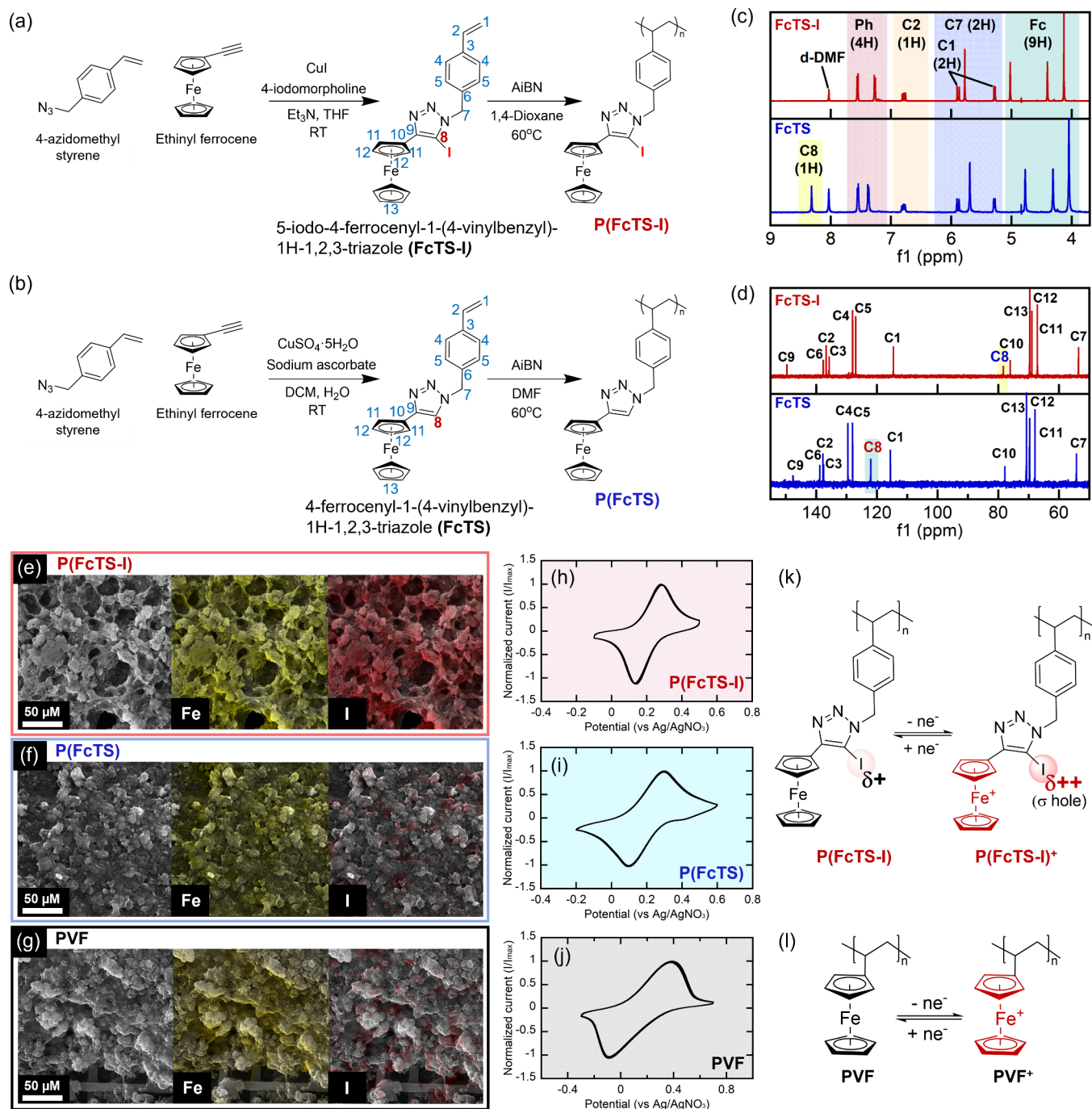
**Figure 1.** Synthesis of redox-active materials. Synthesis of redox-active (a) halogen bonding donor (FcTS-I) and (b) hydrogen bonding donor (FcTS) and their polymer. (c) $^1$H NMR (C$_3$D$_7$NO, 500 MHz) and (d) $^{13}$C NMR (C$_3$D$_7$NO, 125 MHz) spectra of FcTS-I and FcTS. High-resolution SEM images and EDS mapping of (e) P(FcTS-I), (f) P(FcTS), and (g) PVF electrodes. Twenty cycles of cyclic voltammograms of (h) P(FcTS-I), (i) P(FcTS), and (j) PVF electrodes in 100 mM TBAPF$_6$ at a scan rate of 30 mV/s in acetonitrile with activated carbon clothes as a counter and Ag/AgNO$_3$ as a reference electrode. CV plot was normalized by the peak oxidation current ($I/I_{max}$). Electrochemical responses of (k) P(FcTS-I) redox reaction and creation of the sigma hole and (l) PVF redox reaction.

The three ferrocene-based metallopolymers (P(FcTS-I), P(FcTS), and polyvinyl ferrocene (PVF)) were incorporated onto electrodes according to literature protocols.[54,55] To prepare the electrode, carbon nanotubes (CNTs) and redox-active polymers were dispersed at a mass ratio of 0.5:1, along with a 15 wt % cross-linker (1,3-benzenedisulfonyl azide). The introduction of an adequate amount of cross-linker, 1,3-benzenesdisulfonyl azide, allows the formation of cross-links within the polymer film, preventing any dissolution of the

polymer while maintaining consistent uptake performance. The dispersed mixture was then drop-casted onto the electrode substrate and dried at 140 °C to activate the crosslinkers and thus prevent leaching of the organometallic polymer (find detailed methods in Section 4.2). TGA indicates remarkable thermal stability in all three metallopolymers up to 210 °C, supporting that treatment of the electrode at 140 °C does not lead to any polymer degradation (Figure S2.18).
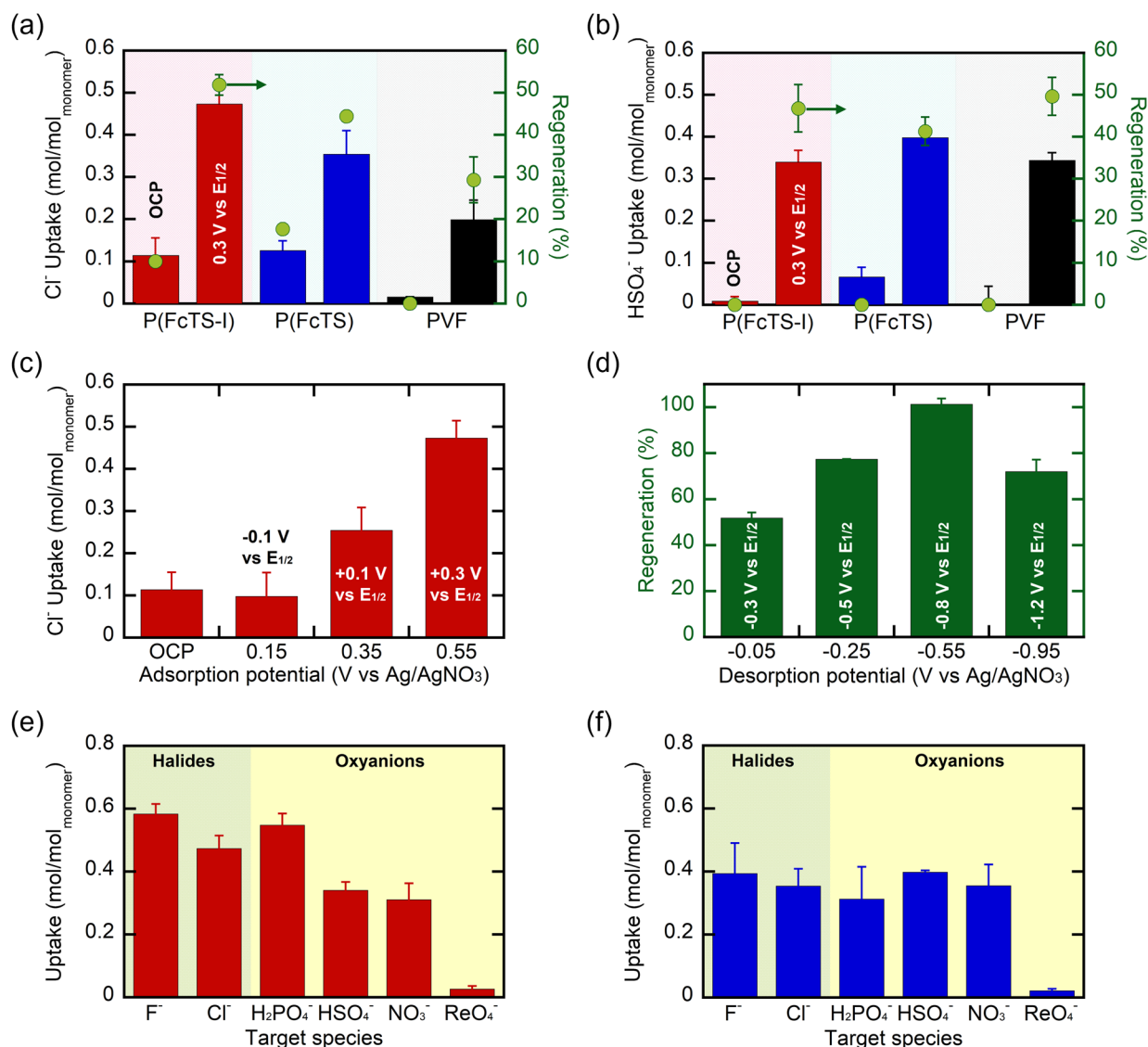
**Figure 2.** Electrochemically reversible electrosorption: electrosorption studies for (a) chloride and (b) bisulfate at open-circuit potential (OCP) and +0.3 V vs $E_{1/2}$ with P(FcTS-I), P(FcTS), and PVF in 1 mM of target anions (in TBA form) and 10 mM TBAPF$_6$ for 15 min, while desorption was performed at the OCP or −0.3 V vs $E_{1/2}$ in 20 mM TBABF$_4$ for 15 min. (c) Adsorption performance of P(FcTS-I) at various potentials from the OCP to 0.55 V vs Ag/AgNO$_3$ (OCP V to 0.3 V vs $E_{1/2}$). (d) Desorption performance of P(FcTS-I) at various potentials from −0.05 to −0.95 V vs Ag/AgNO$_3$ (−0.3 to −1.2 V vs $E_{1/2}$). Electrosorption of various halides (F$^-$, Cl$^-$) and oxyanions (H$_2$PO$_4^-$, HSO$_4^-$, NO$_3^-$, and ReO$_4^-$) with (e) P(FcTS-I) and (f) P(FcTS).

The scanning electron microscopy (SEM) images of ferrocene-based organometallic electrodes (P(FcTS-I), P-(FcTS), and PVF) showed uniform dispersion of the composite on the carbon paper (Figure 1e−g). Energy-dispersive spectroscopy (EDS) mapping images showed a uniform distribution of iron onto the carbon paper. In particular, a one-to-one ratio between iron and iodine contents was observed for the EDS mapping image of P(FcTS-I), which agrees with the elemental analysis results and polymer characterizations shown in SI 2.1.

## 2.2. Electrochemical Characterization of the Redox Polymers

The functionalized redox electrodes are utilized as heterogeneous platforms to study electrochemically reversible halogen bonding, hydrogen bonding, and direct binding onto the ferrocene redox centers. We demonstrated cyclic voltammograms (CVs) of three metallopolymer electrodes to show the reversibility and stability of the redox-active moiety over 20

cycles. In this experiment, we used activated carbon clothes as the counter electrode to avoid any potential impact from high counter potential or solvent degradation. CVs of three metallopolymer electrodes reveal a single oxidation/reduction peak, confirming one electron transfer between ferrocene and ferrocenium (Figure 1h−j). However, $E_{1/2}$ varied with different conjugates on the ferrocene and the values were 0.25, 0.20, and 0.15 V vs Ag/AgNO$_3$ for P(FcTS-I), P(FcTS), and PVF, respectively. A positive shift in the $E_{1/2}$ value often reflects the electron-deficient nature of the ferrocene.[27]

In this regard, the electron-withdrawing triazole and iodine on the P(FcTS-I) thermodynamically disfavored oxidation of the ferrocene moiety by depleting the electron on the ferrocene, resulting in the greatest anodic peak shift of $E_{1/2}$. The downfield shift of ferrocene peaks of FcTs-I on $^1$H NMR spectra by $\delta_{C11} = 0.25$, $\delta_{C12} = 0.09$, and $\delta_{C13} = 0.09$ ppm in comparison to FcTS and by $\delta_{C11} = 0.57$, $\delta_{C12} = 0.15$, and $\delta_{C13} = 0.01$ ppm in

comparison to vinyl ferrocene also supports the electron depletion on ferrocene and positive shift in the $E_{1/2}$ value (Figure 1c and Figures S2.4, S2.9, and S2.14).

CV at varying scan rates from 10 to 100 mV/s showed distinct kinetic behaviors among three metallopolymers (Figures S2.20−2.22). Both P(FcTS-I) and P(FcTS) agree with the Randle−Sevcik equation with a $R^2$ value of >0.99, indicating reversible and diffusion-controlled electron-transfer reactions. In a homogeneous platform, the diffusion limitations of CV originate from the mass transfer of redox species dissolved in the solution. On the other hand, in a heterogeneous platform, these diffusion limitations stem from constrained charge transfers within the film, as well as mass transfer restrictions at the interfaces between the electrode and solution.[56] PVF displayed notable peak splitting between oxidation and reduction reactions, indicating a quasi-reversible system. We believe that the limitations in electron-transfer kinetics may stem from the wide range of molecular weight distribution in PVF, which contains remaining monomers and oligomers (Figures S2.3c and S2.17). This could possibly lead to loosely cross-linked electrodes or uneven distribution of the metallopolymers on the CNTs. Unlike aqueous media, these metallopolymers tend to dissolve in organic media, especially in the presence of loosely bound polymers within a heterogeneous platform or without cross-linker (Figure S2.24). Nevertheless, in the absence of monomers and oligomers, we believe that polymer chain length does not significantly impact the electrochemical properties and overall uptake (Figures S2.25 and S2.26 and Table S2.1). We examined the impact of polymer chain lengths on the uptake performance and found similar chloride uptake for all molecular weights investigated (refer to detailed analysis in SI 2.6). Our study emphasizes the significance of material optimization, such as polymer and electrode synthesis, as well as the judicious design of the electrochemical system to enhance stability.

In the case of P(FcTS-I) and P(FcTS), we expected that the ferrocene moiety would serve as a cooperative binding site to support the binding target species. As an electron-withdrawing group, ferrocene activated the halogen and hydrogen bondings when ferrocene oxidized to ferrocenium ($Fc^+$) (Figure 1k). In the case of P(FcTS-I), oxidized ferrocene redistributed the electron on the iodine, generating an electron-depleted region of $\sigma$-hole for halogen bonding.[19] On the other hand, oxidized ferrocene in PVF served as a direct binding site (Figure 1l), where the cyclopentadienyl group distributed electrons through the $\pi-\pi$ interactions and formed a hydrogen bonding with the anion species.[54]

### 2.3. Electrochemically Reversible Electrosorption Using Redox-Switchable Halogen Bonding

We leveraged XB as a unique supramolecular interaction for selective electrosorption of various anions including halides ($F^-$ and $Cl^-$) and oxyanions ($H_2PO_4^-$, $HSO_4^-$, $NO_3^-$, and $ReO_4^-$) as tetrabutylammonium (TBA) salts (Figure 2a−e). Several of these analytes have been investigated in previous studies to showcase XB interactions.[26,27,57] Thus, the electrosorption trend could indirectly validate the existence of XB interactions in P(FcTS-I) and compare the uptake values with those of P(FcTS) and PVF. To ensure a fair comparison of the electrochemical separation performance among the three different polymers, we adopted the molar ratio (mol of adsorbed target species per mole of monomer unit on the electrode) as the uptake unit for all electrosorption experiments. Given that each monomer unit incorporates one ferrocene (and one iodine/

hydrogen binding site for FcTS-I/FcTS), we expect that there exists one binding site per monomer in all three polymers.

The chloride and bisulfate adsorption tests performed at open-circuit potential (OCP) and 0.3 V (vs $E_{1/2}$) demonstrated the activation of halogen bonding as a result of the oxidation of ferrocene (Figure 2a,b). With the applied potential of 0.3 V versus $E_{1/2}$, the uptake of $Cl^-$ and $HSO_4^-$ using P(FcTS-I) has shown significant enhancement, increasing uptake by factors of 4.2 and 38, respectively, when compared to the OCP. This result underlines the enhancement of the $\sigma$-hole due to the collaborative molecular design of the redox center, as illustrated in Figure 1k. Indeed, this $\sigma$-hole was amplified only following the oxidation of the ferrocene, exhibiting close to OCP uptake of chloride (0.098 mol/mol$_{monomer}$) when applied potential was below $E_{1/2}$ (−0.1 V vs $E_{1/2}$; 0.15 V vs Ag/AgNO$_3$). On the other hand, at applied potentials exceeding $E_{1/2}$ of 0.1 V (0.35 V vs Ag/AgNO$_3$) and 0.3 V (0.55 V vs Ag/AgNO$_3$), notable uptakes of 0.25 and 0.47 mol/mol$_{monomer}$ were observed, respectively (Figure 2c).

Out of the three metallopolymers, P(FcTS-I) exhibited the highest halide uptake of 0.58 mol/mol$_{monomer}$ for fluoride and 0.47 mol/mol$_{monomer}$ for chloride. This observation indicates a strong XB affinity toward halide species in comparison to HB observed with P(FcTS) (0.39 mol/mol$_{monomer}$ and 0.35 mol/mol$_{monomer}$) or PVF (0.31 mol/mol$_{monomer}$ and 0.20 mol/mol$_{monomer}$) for fluoride and chloride, respectively (Figure 2e,f and Figure S3.1). Among oxyanions, P(FcTS-I) demonstrated 175 and 287% enhanced phosphate uptake of 0.55 mol/mol$_{monomer}$ compared to P(FcTS) (0.31 mol/mol$_{monomer}$) and PVF (0.19 mol/mol$_{monomer}$), respectively. Furthermore, a similar uptake was observed for $HSO_4^-$ and $NO_3^-$ among the three metallopolymers. Interestingly, metal oxyanions (perrhenate and $ReO_4^-$) did not bind with either P(FcTS-I) or P(FcTS) while PVF exhibited significant uptake of $ReO_4^-$ (0.24 mol/mol$_{monomer}$). The uptake trend observed for P(FcTS-I) is consistent with findings from previous sensing studies.[26,45,58] Many of these studies indicated that the charge density and electronegativity of the XB acceptors significantly affect the strength of XB interactions, while partial steric hindrance and solvent interaction may influence the overall uptake trend, especially for bulky target molecules.[22,59,60] We observed exclusive uptake of target species for all ferrocene-based organometallic polymers despite the presence of 10 times excess $PF_6^-$ in the solution. The negative charge of $PF_6^-$ is evenly distributed among its six fluorine atoms, exhibiting low electron density for each fluorine atom.[61] Consequently, the weak atomic partial charges of fluoride lead to low binding affinity toward the metallopolymer, resulting in highly selective uptake of target species with (halides and oxyanions) over $PF_6^-$.

To study the switch-off capability of XB, we demonstrated the desorption test for chloride and bisulfate at a reversal potential of −0.3 V vs $E_{1/2}$. P(FcTS-I) released 57 and 52% of the bound chloride and bisulfate, resulting in a 5.7-fold increase in regeneration compared to the onset of the OCP (Figure 2a,b). Additionally, P(FcTS-I) exhibited a 34% higher regeneration performance on average than both FcTS and PVF. At an even higher negative potential of −0.8 V vs $E_{1/2}$, the weak $\sigma$-hole between P(FcTS-I) and chloride was completely deactivated, resulting in the release of 100% of the bound chloride (Figure 2d). However, applying a more negative potential (−1.2 V vs $E_{1/2}$) led to a decrease in regeneration down to 72% due to the chlorine generations on the counter electrode (Figure 2d and Figure S3.3).
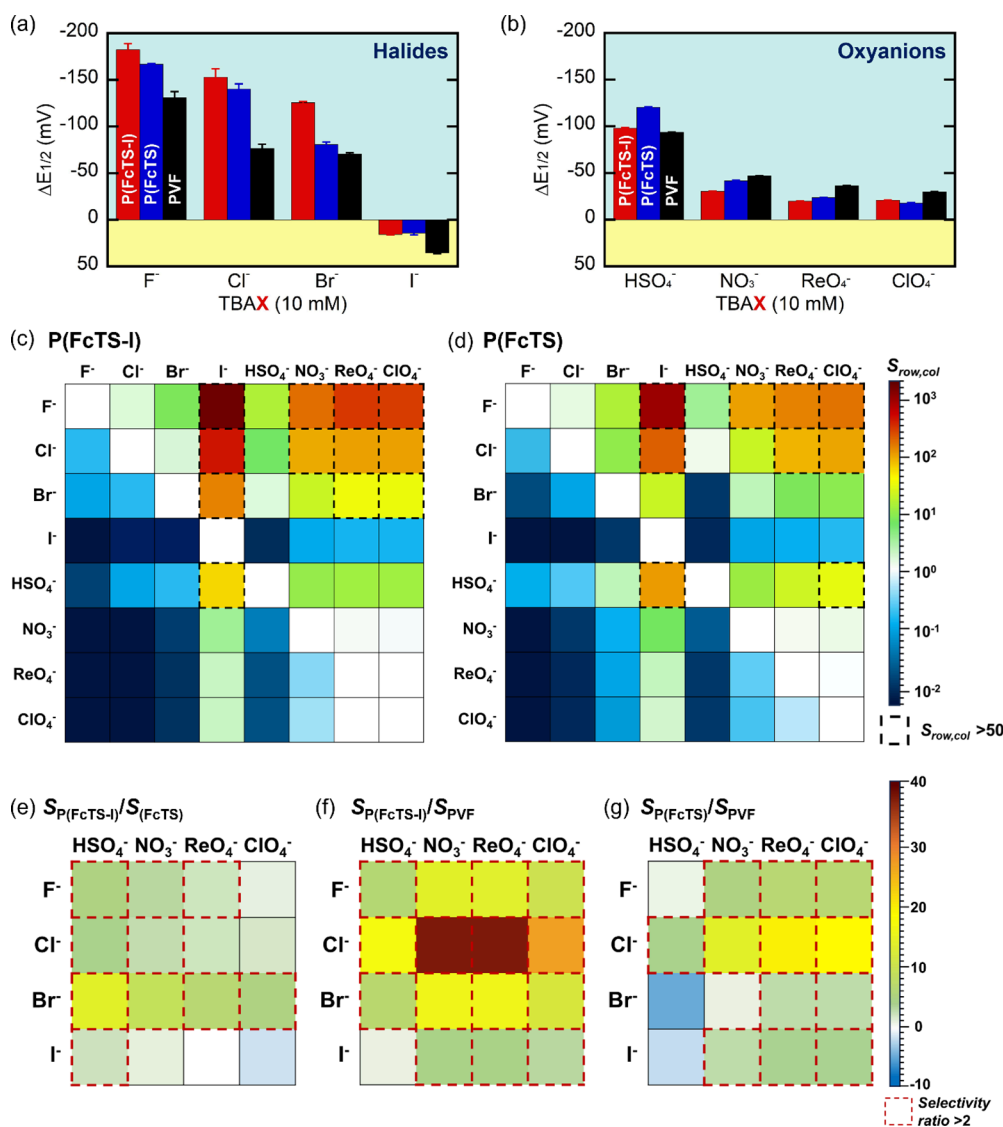
**Figure 3.** Anion recognition studies and thermodynamic selectivity assessment: peak shift values ($\Delta E_{1/2}$) of (a) halides ($F^-$, $Cl^-$, $Br^-$, and $I^-$) and (b) oxyanions ($HSO_4^-$, $NO_3^-$, $ReO_4^-$, and $ClO_4^-$). $\Delta E_{1/2}$ was calculated by the $E_{1/2}$ peak shift in CV after the addition of 10 mM target anions at a scan rate of 30 mV/s. Heat map of thermodynamic selectivity across varied target halides and oxyanions for (c) P(FcTS-I) and (d) P(FcTS). Heat map of selectivity ratio for the selectivity values of halides versus oxyanions between (e) P(FcTS-I) and P(FcTS), (f) P(FcTS-I) and PVF, and (g) P(FcTS) and PVF. Thermodynamic selectivity was determined based on the anion recognition results ($\Delta E_{1/2}$), while the selectivity ratio was calculated by dividing the thermodynamic selectivity of one polymer by that of the other polymer. In (c) and (d), separation factors over 50 were indicated with a dotted border, while selectivity ratios over 2 were denoted with a red-dotted border in (e–g).

On top of the desorption capability, we performed long-term charging/discharging tests to demonstrate the stability and redox switchability of P(FcTS-I) over 200 cycles (Figures S3.4 and S3.5). Charging and discharging capacities were maintained at 88 and 87% respectively, over 200 cycles with an overall Coulombic efficiency above 99%, emphasizing the high electrochemical stability and reversibility of P(FcTS-I). Overall, the adsorption and desorption tests, along with the long-term cycle operation, demonstrate the switchable nature of halogen bonding by controlling the strength of the redox-active electron-withdrawing group, ferrocene.

### 2.4. Selective Inorganic Anion Recognition and Thermodynamic Selectivity Analysis

In addition to the electrosorption test, we examined the electrochemical sensing responses of P(FcTS-I), P(FcTS), and PVF toward a range of inorganic anions, including halides

($F^-$, $Cl^-$, $Br^-$, and $I^-$) and oxyanions ($H_2PO_4^-$, $HSO_4^-$, $NO_3^-$, $ReO_4^-$, and $ClO_4^-$) to access the correlation between anion recognition and electrosorption trends (Figure 3a,b). The overall uptake pattern of both halide and oxyanions shown in Figure 2 and Figure S3.1 aligns with the sensing trends shown in Figure 3a,b and is also in line with previous studies on redox-active XB sensors.[26,45,58] P(FcTS-I) exhibited a 10% enhancement in fluoride recognition ($\Delta E_{1/2}$ = −182 mV) and chloride recognition ($\Delta E_{1/2}$ = −153 mV) compared to P(FcTS), while a 78% greater peak shift ($\Delta E_{1/2}$) was observed for chloride and bromide ($\Delta E_{1/2}$ = −140 mV) compared to PVF (Figure 3a and Table S3.1). This result highlights the presence of strong XB intermolecular interactions between σ-hole on the P(FcTS-I) and target anions. The strength of XB with XB donor molecules (P(FcTS-I) in our study) is largely influenced by the electronegativity of the XB acceptor (target anions),[19] which in turn correlates with charge density[62] and basicity.[63] Thus, the
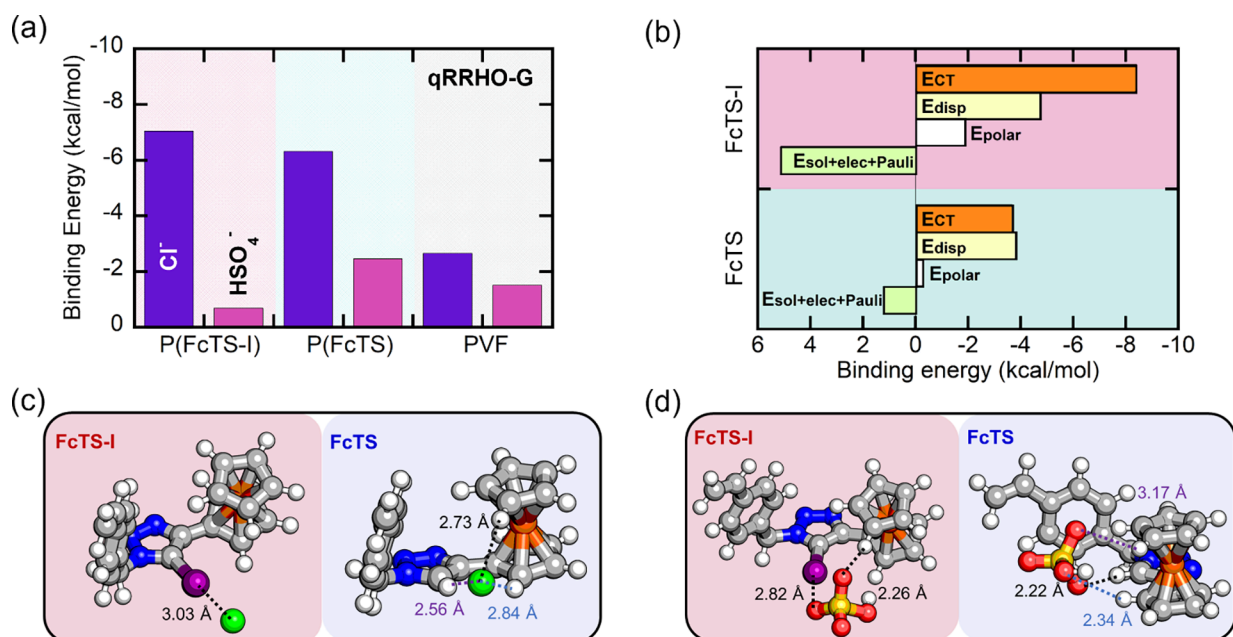
**Figure 4.** Binding mechanism investigation through DFT calculations: (a) Binding energies ($\Delta G$) of $Cl^-$ and $HSO_4^-$ to oxidized P(FcTS-I), P(FcTS), and PVF in acetonitrile solvent. Temperature corrections are calculated by the qRRHO-G method with the 150 cm$^{-1}$ cutoff. (b) Energy decomposition of $[FcTS-I]^+-Cl^-$ and $[FcTS]^+-Cl^-$, where $E_{CT}$ (orange), $E_{disp}$ (yellow), $E_{polar}$ (white), and $E_{sol+elec+Pauli}$ (green) represent charge transfer, dispersion, polarization, and solvation+electrostatic+Pauli repulsion energies, respectively. Illustrations of optimized structures of (c) $[FcTS-I]^+-Cl^-$ and $[FcTS]^+-Cl^-$ and (d) $[FcTS-I]^+-HSO_4^-$ and $[FcTS]^+-HSO_4^-$ at the $\omega$B97X-D3(BJ)/ma-def2-TZVP level of theory in acetonitrile, where atoms are shown using the ball and stick model with C in gray, H in white, N in blue, Fe in orange, Cl in green, O in red, and S in yellow.

trend of electrochemical sensing response follows the electronegativity of the halides ($F^- > Cl^- > Br^- > I^-$) for all redox-active metallopolymers. Despite the potential for bromide and iodide to form trihalides, there is no indication of additional peaks corresponding to interactions between the polymer and $X_3^-$. Instead, a slight anodic peak shift was observed for $I^-$ due to its weaker electronegativity, resulting in a binding interaction that is similar to or even less favorable than that of the electrolyte ($PF_6^-$). Moreover, the standard reduction potential of iodide is 0.34 V vs Ag/Ag$^+$,[64] which is close to the oxidation of ferrocene (0.3–0.6 V vs Ag/Ag$^+$). The proximity of oxidation potential values leads to iodide oxidation as a side reaction of ferrocene oxidation, ultimately resulting in weaker anion recognition.

Of oxyanions, $HSO_4^-$ revealed the strongest sensing response of $\Delta E_{1/2} = -98$ mV toward P(FcTS-I), followed by $NO_3^-$ ($-30$ mV), $ClO_4^-$ ($-21$ mV), and $ReO_4^-$ ($-20$ mV) (Figure 3b and Table S3.1). Note that $\Delta E_{1/2}$ values for phosphate monobasic ($H_2PO_4^-$) could not be determined due to its varying speciation between $HPO_4^{2-}$ and $H_2PO_4^-$ under the present solvent conditions, which results in more than one oxidation and reduction peaks (Figure S3.6). Oxyanions, which have relatively low charge density compared to halides, interacted with P(FcTS-I) through weak XB interactions incorporated with the strong HB interactions between oxygens on the oxyanions and hydrogen atoms on the cyclopentadienyl ring (as further discussed in Section 2.5).

Based on the peak shift values, we analyzed thermodynamic selectivity across varied target halides and oxyanions and illustrated them as heat maps in Figure 3c–g and Figure S3.7 (find detailed methods in SI 3.3). P(FcTS-I), P(FcTS), and PVF exhibited greater affinity toward halides ($F^-$, $Cl^-$, and $Br^-$) compared to oxyanions ($HSO_4^-$, $NO_3^-$, $ReO_4^-$, and $ClO_4^-$) with the selectivity value range from 0.22 to 560 (Figure 3c,d and Figure S3.7). However, iodine showed notably low selectivity for

all three polymers, due to its low electronegativity and oxidation potential close to the ferrocene. Additionally, interactions with $HSO_4^-$ were stronger than those with $Br^-$ for P(FcTS) and $Cl^-$ and $Br^-$ for PVF, resulting in selectivity values below 1 ($S_{P(FcTS)}$ of 0.21 for $Cl^-$ vs $HSO_4^-$; $S_{PVF}$ of 0.51 and 0.41 for $Cl^-$ vs $HSO_4^-$ and $Br^-$ vs $HSO_4^-$, respectively (Figure 3d and Figure S3.7). In particular, among the three polymers, P(FcTS-I) displayed the highest selectivity for halides over oxyanions. Consequently, among 12 binary mixtures, involving $F^-$, $Cl^-$, and $Br^-$ against $HSO_4^-$, $NO_3^-$, $ReO_4^-$, and $ClO_4^-$, eight surpassed selectivity values of 50 (indicated with a dotted border) for P(FcTS-I), whereas P(FcTS) and PVF decreased to 5 and 1, respectively (Figure 3c,d and Figure S3.7), highlighting the importance of selective halogen bonding interactions between P(FcTS-I) and halides.

To assess the selectivity among polymers, we calculated the selectivity ratio by dividing the selectivity of one polymer by that of another polymer for halides versus oxyanions (Figure 3e–g). Comparing P(FcTS-I) with P(FcTS), P(FcTS-I) demonstrated superior halide selectivity, yielding selectivity ratios ($S_{P(FcTS-I)}/S_{P(FcTS)}$) up to 13.62 (with an average of 3.8) (Figure 3e). Moreover, we observed selectivity ratios ($S_{P(FcTS-I)}/S_{PVF}$) exceeding 37, with an average selectivity ratio of 14, between P(FcTS-I) and PVF (Figure 3f). Given that this selectivity ratio reached only up to 19, with an average selectivity ratio of 5.9 between P(FcTS) and PVF (Figure 3g), thermodynamic selectivity analysis underscores that XB-based supramolecular interactions tend to show a preference for halide bindings, resulting in increased uptake, as well as selectivity.

Although there is a similar trend between anion recognition and uptake, the values for uptake cannot be quantitatively compared with the sensing trend. For instance, the thermodynamic selectivity values of P(FcTS-I) between chloride and oxyanions (e.g., $HSO_4^-$, $NO_3^-$, and $ReO_4^-$) exhibit 3.2-fold
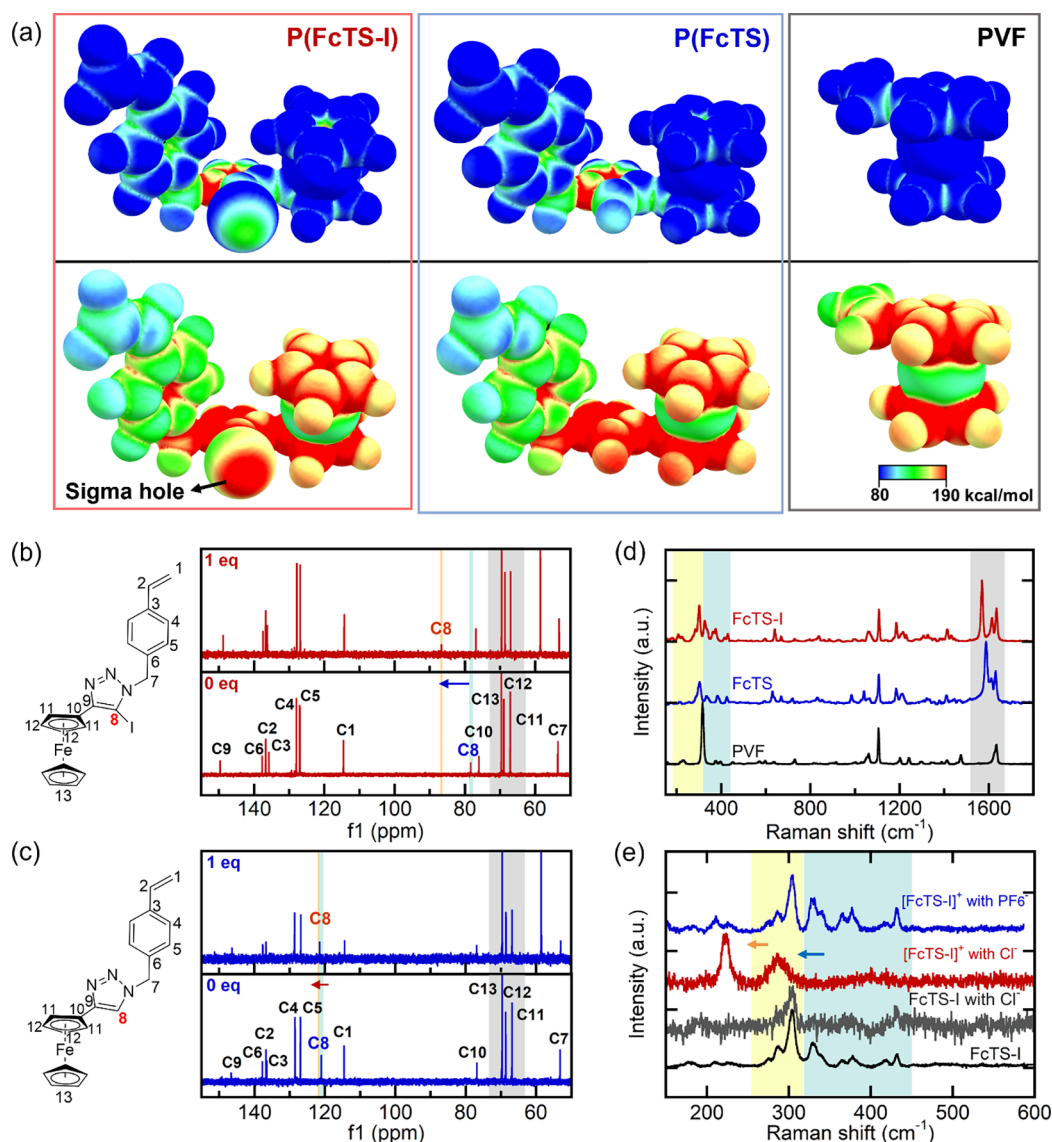
**Figure 5.** Spectroscopic and computational investigations of halogen bonding interactions: (a) Molecular electrostatic potential surface (ESP) mapping at an isovalue of 0.3 au for reduced (top) and oxidized (bottom) states of P(FcTS-I), P(FcTS), and PVF. ESP was generated using the mapped vdW spheres with the scale value of 0.85 and the potential between 80 and 190 kcal/mol. $^{13}$C NMR ($C_3D_7NO$, 125 MHz) spectra of (b) FcTS-I and (c) FcTS in the presence of 0 and 1 equiv of TBACl. Ex-situ Raman spectra of (d) FcTS-I, FcTS, and vinyl ferrocene and (e) reduced and oxidized FcTS-I in the presence of 10 mM Cl$^-$ and oxidized FcTS-I in the presence of 10 mM of PF$_6^-$. The electrochemical oxidation for ex-situ Raman was done in a homogeneous phase, dissolving 5 mM FcTS-I in acetonitrile and applying 0.3 V vs $E_{1/2}$ for 30 min.

greater selectivity values than those obtained from binary electrosorption tests (Figure S3.8). The difference arises from the fact that the electrosorption process is not solely determined by the binding affinity of the target species, as measured by the peak shift analysis. It is also significantly influenced by the concentration of the target species and competing ions (in this case, PF$_6^-$), applied potential, and oxidation time.[10] We observed exclusive uptake of target species for all ferrocene-based organometallic polymers, despite the presence of 10 times excess PF$_6^-$ in the solution. Consequently, the weak atomic partial charges of fluoride lead to low binding affinity toward the metallopolymer, resulting in highly selective uptake of target species with (halides and oxyanions) over PF$_6^-$.

## 2.5. Mechanistic Understanding of Selective Electrosorption through Density Functional Theory Calculations

We conducted DFT calculations to understand the binding mechanism for selective electrosorption and deconvolute the potential role of halogen bonding from the redox-active motif. The $\Delta G$ trend aligned with the sensing and uptake results, showing [P(FcTS-I)]$^+$-Cl$^-$ the highest $\Delta G$ value of −7.04 kcal/mol compared to those of [P(FcTS)]$^+$-Cl$^-$ ($\Delta G$ = −6.31 kcal/mol) and PVF$^+$-Cl$^-$ ($\Delta G$ = −2.65 kcal/mol) (Figure 4a). In particular, the binding energy for chloride on [P(FcTS-I)]$^+$ was significantly stronger than that of bisulfate ($\Delta G$ = −0.68 kcal/mol), which confirms the preferential sorption of chloride through XB interactions. The robust binding between XB donor species and chloride is a result of the directional nature of the binding interactions (Figure 4c and Figure S4.2) and the orbital overlap configuration between the two (Figure S4.7). The

binding between P[FcTS-I]$^+$ and Cl$^-$ has a linear orientation with a bond length of 3.03 Å and a [C−I]-Cl$^-$ angle of 178.5° (Figure 4c). However, the binding between P[FcTS-I]$^+$ and HSO$_4^-$ involves a more intricate series of interactions through partial halogen and hydrogen bonding interactions with more than one oxygen atom of HSO$_4^-$. These interactions entail a partial halogen bonding between the oxygen atom and iodine on FcTS-I with a bond length of 2.82 Å as well as a partial hydrogen bonding between another oxygen atom and hydrogen on the cyclopentadienyl ring with a bond length of 2.26 Å (Figure 4d). Hydrogen atoms on the cyclopentadienyl ligand serve as hydrogen bonding donors, forming robust interactions with the target species, as demonstrated in earlier studies.[10,54,65] The optimal binding configuration emphasizes the synergistic role of halogen bonding with hydrogen bonding interactions in the electrosorption of oxyanions. By calculating the electron density ($\rho$) at the bond critical point (see SI 4.3 for detailed analysis), we confirmed that the excess electron in the p$_z$ orbital of chloride allows for direct interaction with the sigma hole of iodine. On the other hand, the excess electron in the bisulfate anion is present in the highest occupied molecular orbital, resembling the p-orbitals of oxygen atoms. This arrangement results in the formation of noncovalent bonds with iodine, contributing to a comparatively weaker interaction (Figures S4.7b and S4.9). Both the molecular-level binding mechanism and experimental observations indicate that several factors influence the binding affinity, including not only the electronegativity of the species but also the molecular structure, charge density and distribution, basicity, competing ions, and solvent.

The nature of the interaction between Cl$^-$ and HSO$_4^-$ and between oxidized FcTS-I and FcTS molecules was further probed through energy decomposition analysis (Figure 4b and Figure S4.12). The result shows that the charge transfer interaction serves as the primary contributor in stabilizing the [P(FcTS-I)]$^+$-Cl$^-$ system with an energy of −8.41 kcal/mol. This strong charge transfer interaction between the filled orbital of chloride and the unoccupied orbital localized on iodine indicates the presence of XB in chloride binding, as evidenced by the complementary occupied and virtual pair orbital (COVP) analysis (Figure S4.10a). Both occupied chloride orbital and unoccupied iodine orbitals are directed toward each other and aligned along the same axis, resulting in a directional halogen bonding. The binding strength and stability of the complex molecule are further enhanced through the synergistic effects of dispersion and polarization with the charge transfer, while the combination of solvation, electrostatic, and Pauli repulsion energies ($E_{sol+Elec+Pauli}$) exerts a counteractive effect on the binding of chloride to the oxidized P(FcTS-I), largely due to the high positive solvation energy.

In the absence of directional XB, weak binding interactions were observed within the complex molecule. The COVP orbitals in the [P(FcTS)]$^+$-Cl$^-$ system revealed that occupied orbitals localized on chloride and virtual pairs were distributed over C−H bonds of triazole and the cyclopentadienyl ring (Figure S4.11a), resulting in relatively weak charge transfer and dispersion interactions between [P(FcTS)]$^+$-Cl$^-$ compared to [P(FcTS-I)]$^+$-Cl$^-$ (Figure 4b). The energy decomposition analysis for bisulfate binding also showed that dispersion is the dominant interaction of both [P(FcTS-I)]$^+$ and [P(FcTS)]$^+$ (Figure S4.12), followed by charge transfer, which is in agreement with the bond critical points analysis (Figures S4.7 and S4.8). In particular, the prevalent dispersion interactions arising from multiple HBs between bisulfate and hydrogen

atoms on the cyclopentadienyl ring weakened the selective XB interactions of P(FcTS-I) and led to a binding mechanism and uptake similar to that of P(FcTS). Overall, the calculated binding energy and energy decomposition analyses align with the observed uptake trends and anion recognition results in Figures 2 and 3, emphasizing the relatively weaker nature of halogen bonding interactions with oxyanions compared to halides.

## 2.6. Spectroscopic and Computational Investigations to Support the Existence of Halogen Bonding Interactions

The existence of the XB interaction can be confirmed experimentally through NMR and Raman studies in addition to molecular electrostatic potential surface (EPS) mapping. EPS mapping of FcTS-I illustrates the remarkable delocalization of the excess positive charge, especially on the iodine, compared to the hydrogen(s) on the triazole motif in FcTS and cyclopentadienyl ring in the PVF (Figure 5a). The strong positive potential (105 kcal/mol) on the iodine atom indicates the presence of the $\sigma$-hole in the oxidized state of FcTS-I, while a slightly weak positive potential (39.1 kcal/mol) is still present in the neutral state (Figure S4.13a). This electrostatic potential near the surface of the $\sigma$-hole reached up to 190 kcal/mol upon the oxidation of ferrocene (Figure 5a). On the other hand, FcTS and vinyl ferrocene molecules involve lower positive potentials distributed among hydrogens in the triazole and cyclopentadienyl group than $\sigma$-hole, resulting in a weaker interaction between target species and hydrogen atoms than halogen bonding.

The strength of the XB interaction can be measured by NMR titration in a neutral ferrocene state. A notable downfield shift ($\delta$ = 8.32 and 9.23 ppm) of iodine-bound carbon (C8 for FcTS-I) was witnessed in the presence of 1 and 2 equiv of Cl$^-$, respectively (Figure 5b and Figure S5.1). This distinct peak shift of C8 in FcTS-I indicates the presence of halogen bonding (I−Cl$^-$), which weakens the heavy atom effect. For FcTS-I, C8 was originally upfield-shifted (Figure 1d) as the iodine atom shared its electron with the adjacent light atom (C8) by the spin−orbital coupling, known as the heavy atom effect.[53,66,67] When this heavy atom forms a halogen bonding with the Lewis base (Cl$^-$), the electron shielding effect on the light atom becomes weak, resulting in a downfield shift in $^{13}$C NMR. On the other hand, the presence of 1 and 2 equiv of PF$_6^-$ did not result in any significant peak shift due to its weak binding affinity toward $\sigma$-hole (Figures S5.6−S5.7). This result aligns with the electrosorption and anion recognition results, which indicate a preferential molecular interaction with halides and oxyanions compared to PF$_6^-$. Moreover, an insignificant shift ($\delta$ = 0.45 ppm) in the C8 peak of FcTS upon the addition of 1 and 2 equiv of Cl$^-$ (Figure 5c and Figure S5.2) highlights the presence of a sigma hole on the iodide of FcTS-I, serving as a binding site for Cl$^-$. Additionally, among the three studied organometallic species, no significant peak shift was observed in the $^{13}$C NMR and $^1$H NMR spectra corresponding to the cyclopentadienyl rings, which suggests that there is a lack of hydrogen bonding between ferrocene and chloride when ferrocene is in a reduced state (Figures S5.1−S5.7).

To assess the halogen bonding ability of oxidized FcTS-I, ex-situ Raman spectroscopy was performed since the paramagnetic nature of iron makes it difficult to examine the peak shift of ferrocene-containing molecules through NMR.[54,66] Prior to analyzing structure changes in FcTS-I, we verified two distinct regions in its Raman spectra (150−450 and 1530−1680 cm$^{-1}$)
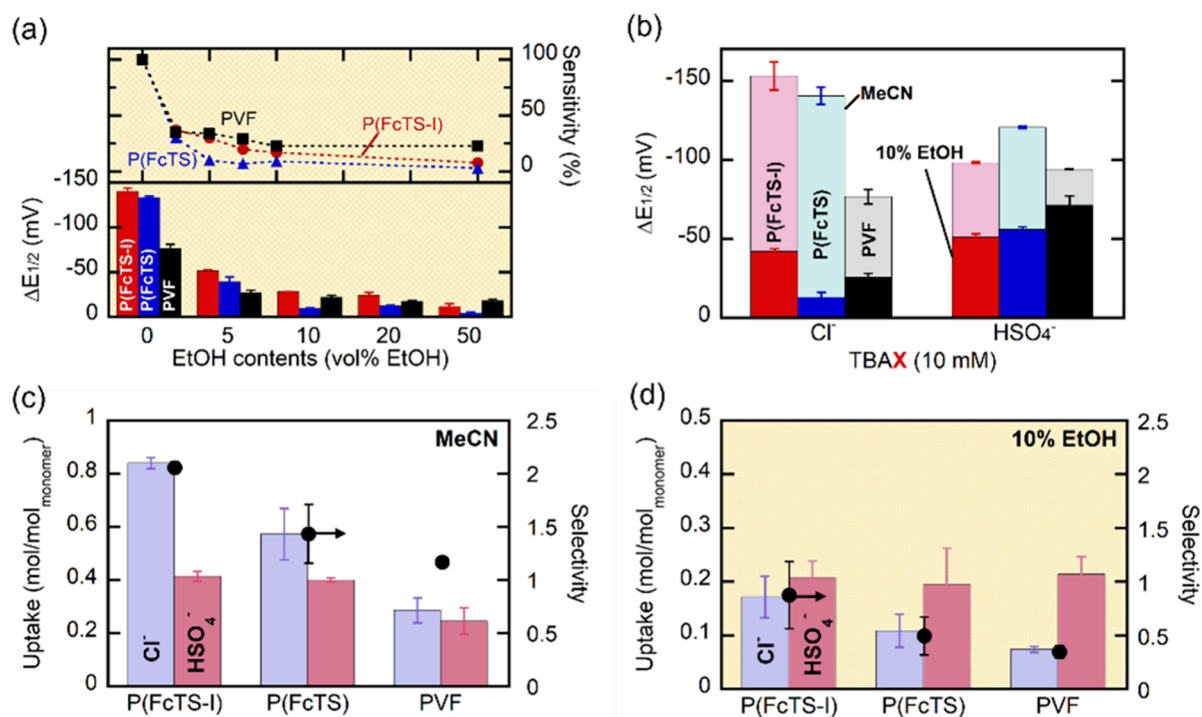
**Figure 6.** Anion recognition and electrosorption performance in the presence of the protic solvent. (a) Chloride recognition with respect to the addition of ethanol in the solvent. (b) Sensing capability toward chloride and bisulfate in acetonitrile (shaded) and in 10:90 vol % of ethanol:acetonitrile (colored). Chloride and bisulfate uptakes (c) in acetonitrile and (d) in 10:90 vol % of ethanol:acetonitrile. The electrosorption was carried out at +0.3 V versus $E_{1/2}$ in 5 mM Cl$^-$ and 5 mM HSO$_4^-$ for 15 min. The selectivity was calculated by $S_{chloride}$ = ([Cl$^-$]$_{ads}$/[HSO$_4^-$]$_{ads}$)/ ([Cl$^-$]$_{sol}$/[HSO$_4^-$]$_{sol}$) in mol.

compared to FcTS and PVF (Figure 5d). Then, DFT calculations confirmed that the observed peak regions, specifically below 400 cm$^{-1}$ in the Raman spectrum, correspond to C−I motions, including strong C−I bending and stretching at 223, 269, 299, and 419 cm$^{-1}$ (Figure S5.8 and Figure S5.9). During the oxidation of FcTS-I, the halogen bonding was accompanied by the downfield shift at low Raman shift regions with very broad signals, presumably originating from the increased bond length of C−I after the formation of the I−Cl$^-$ bond (Figure 5e). The Raman peak shift was not noticeable when FcTS-I was in its neutral state with chloride due to the weak interaction between the σ-hole and anion. Unlike $^{13}$C NMR, where individual peak corresponds to specific carbon atoms (e.g., carbon on iodine, C8) within the FcTS-I molecule, Raman spectroscopic peaks represent the collective molecular bond vibrations of the entire FcTS-I molecule (Figure S5.9). Consequently, in a neutral state of FcTS-I, the weak XB interaction did not significantly alter the overall molecular bond vibrations of FcTS-I. Furthermore, even upon the oxidation of FcTS-I, PF$_6^-$ did not cause any observable shift in the Raman peaks. This observation confirms halogen bonding serving as the primary binding site in the selective interaction between P(FcTS-I) and chloride, with the ferrocene motif acting as a secondary, synergistic binding site in the electrochemically responsive binding.

### 2.7. Effect of the Protic Solvent on Sensing Capabilities and Selectivity of Halogen Bonding

The exceptional anion recognition properties of halogen bonding and its electrosorption can be observed, even in a mixed volume percentage of water and ethanol (Figure 6). Halogen bonding outperformed the anion recognition with peak shift values of −24 and −20 mV, for mixtures containing less

than 20 vol % ethanol and 10 vol % water, respectively (Figure 6a and Figure S3.9). On the other hand, the sensing capabilities of P(FcTS) were minimal in the mixtures containing 10 vol % ethanol and water. In a protic mixture, the solvent can serve as an alternative medium for stabilizing the redox-active unit,[26,29] decreasing the sensing abilities of both halogen and hydrogen bonding due to the solvation effect and solvent interaction. In this context, P(FcTS) and PVF favor stabilizing ferrocenium by forming hydrogen bonds with the protic solvent mixture while P(FcTS-I) still prefers binding chloride through halogen bonding to stabilize the ferrocenium. This result underscores that redox-mediated XB can partially alleviate the inherent challenges associated with XB interactions in polar protic solvents. XB often encounters difficulty in interacting with target species in polar protic solvents due to competitive hydrogen bonding interactions between target species and polar solvents, or between XB donors and polar solvents.[68] With the creation of a strong electron-withdrawing group upon oxidation, redox-active XB donor species have demonstrated the capability to partially alleviate these intrinsic challenges of XB by overcoming solvent interactions in protic media.[26,45] While fully implementing XB in polar solvents remains a considerable challenge, we believe that redox-mediated XB provides a strategy to mitigate the inherent limitations of XB.

The binding affinity was significantly influenced by the solvation of the anions, resulting in noticeable changes in the overall uptake. The chloride uptake performance of P(FcTS-I) exhibited a 48% decrease in the presence of 10 vol % ethanol when compared to a pure acetonitrile solution (Figure S3.10). The decrease in uptake performance can be attributed to the solvation of chloride ions in the 10 vol % ethanol solution. Interestingly, depending on the countercations, this uptake
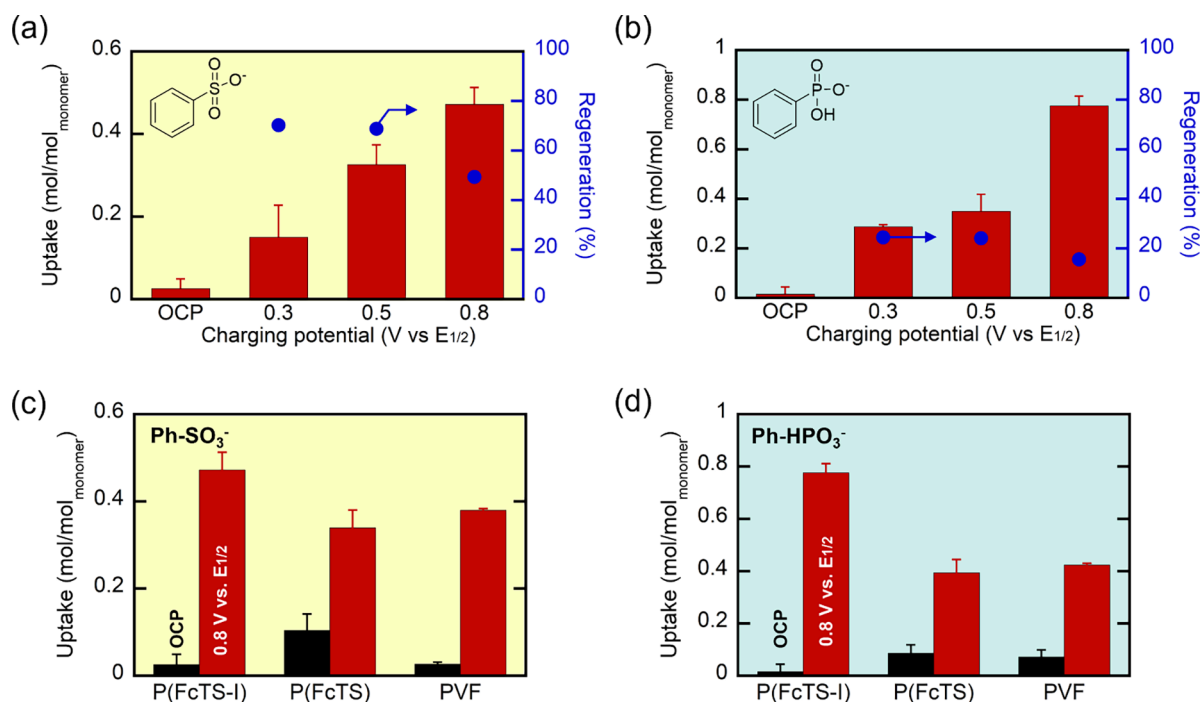
**Figure 7.** Redox electrosorption of organic compounds: The adsorption capacity of (a) benzenesulfonate (Ph-SO$_3^-$) and (b) phenyl phosphonate (Ph-HPO$_3^-$) at various electrosorption potentials from the open-circuit potential (OCP) to $\pm 0.8$ V vs $E_{1/2}$. The adsorption capacity of (c) benzenesulfonic acid (Ph-SO$_3^-$) and (d) phenyl phosphonic acid (Ph-HPO$_3^-$) with P(FcTS-I), P(FcTS), and PVF at $\pm 0.8$ V vs $E_{1/2}$. The adsorption was performed in 1 mM Ph-HSO$_3$ and Ph-H$_2$PO$_3$ and 10 mM TBAPF$_6$ as a supporting salt for 15 min, while desorption was performed in 20 mM TBABF4 for 15 min.

trend may vary due to ion dissociation (Figure S3.10). For example, LiCl, which is hardly dissociable in pure acetonitrile,[69] resulted in a 72% reduction in chloride uptake in comparison to TBACl, whereas in the presence of 10% ethanol, the impact of countercations seems to be less significant, leading to only a 40% reduction in chloride uptake compared to TBACl.

Furthermore, the solvent interactions also alter the selectivity patterns for anion recognition and electrosorption. In the 10 vol % ethanol mixture, anion recognition showed a reversed trend, with a 70−90% decrease in peak shift for chloride but only 24−54% for bisulfate (Figure 6b). The addition of ethanol also altered the uptake preference from chloride to bisulfate (Figure 6c,d). In pure acetonitrile, P(FcTS-I) showed the highest selectivity toward chloride with a selectivity of 2.1, surpassing the selectivity values for P(FcTS) (1.4) and PVF (1.8). However, in the 10 vol % ethanol mixture, the three metallopolymers showed a higher affinity toward bisulfate, leading to a selectivity range of 0.35−0.87. The change in the selectivity patterns can be attributed to distinct solvation behaviors of chloride and bisulfate. Chloride exhibits a higher degree of hydration, with six water molecules in a protic solvent, compared to bisulfate, which can be stabilized with one to four water molecules.[70,71] Thus, chloride stabilizes with the interaction of protic solvent, resulting in a weaker interaction between chloride and the oxidized organometallic species than that of bisulfate. The reversal selectivity trend across P(FcTS-I), P(FcTS), and PVF, regardless of bonding type, implies that this trend is driven by the solvation of target species rather than changes in organometallic properties in the presence of a protic solvent. Overall, electrosorption results highlight that the selectivity can be controlled by the design of molecularly selective electroactive materials as well as by modulating the solvent mixture.

## 2.8. Redox-Switchable Halogen Bonding for the Recovery of Organic Molecules

P(FcTS-I) exhibited remarkable electrosorption of organic species, thereby expanding the potential for XB-based electrochemical separations from halides and oxyanions to include more valuable species found in nonaqueous media. We selected benzenesulfonate (Ph-SO$_3^-$) and phenyl phosphonate (Ph-HPO$_3^-$) as representative organic species (Figure 7) due to their extensive application in chemical production[72] and pharmaceuticals,[73] as well as the widespread utilization of their numerous derivatives. As shown in the adsorption of inorganic species, a weak binding interaction was present at the OCP, resulting in insignificant uptake values of 0.026 and 0.016 mol/mol$_{monomer}$ for Ph-SO$_3^-$ and Ph-HPO$_3^-$, respectively (Figure 7a,b). Out of the three metallopolymers studied, P(FcTS) displayed the highest uptake for both Ph-SO$_3^-$ and Ph-HPO$_3^-$ at the OCP with uptake values of 0.105 and 0.086 mol/mol$_{monomer}$, respectively. This can be attributed to the inherent partial oxidation of P(FcTS), as shown in the OCP profiles and XPS spectra of Fe 2p (Figures S3.11 and S2.19). As the applied potential increased from the OCP to 0.8 V versus $E_{1/2}$, both uptake values of Ph-SO$_3^-$ and Ph-HPO$_3^-$ for P(FcTS-I) were 18 and 49 times enhanced, emphasizing the electrochemically responsive binding of P(FcTS-I) with charged organic species. Up to 70% of Ph-SO$_3^-$ was released with a reversal potential, whereas only up to 25% of Ph-HPO$_3^-$ was released due to its strong binding with P(FcTS-I), as confirmed by LSV results (Figure S3.12). Therefore, additional improvements to the operational parameters are required to enhance electrosorption and its reversibility.

Furthermore, we compared the uptake performance of P(FcTS-I) with P(FcTS), and PVF as illustrated in Figure 7c,d. P(FcTS-I) exhibited 39 and 24% greater uptake of Ph-

$SO_3^-$ (0.43 mol/mol$_{monomer}$) than P(FcTS) (0.31 mol/mol$_{monomer}$) and PVF (0.34 mol/mol$_{monomer}$). In addition, we obtained a twofold enhanced uptake of Ph-HPO$_4^-$ with our halogen bonding donor molecule (0.71 mol/mol$_{monomer}$) compared to P(FcTS) and PVF (0.36 and 0.39 mol/mol$_{monomer}$, respectively). This result demonstrates the capability of halogen bonding for separating diverse charged molecules in organic media, thus expanding the application scope toward pharmaceutical and chemical synthesis processes. Acknowledging the complex surface charge distribution of organic species, it is evident that multiple binding interactions occur between the metallopolymer and the organic species. Thus, we believe that conducting larger scale DFT calculations and molecular dynamics simulations will be essential for gaining a comprehensive understanding of the macromolecular binding effects between organic species and halogen-bonding donor polymers. Overall, electrochemically responsive halogen bonding offers a paradigm shift in separation technology. It enables the fine-tuning of bonding strength through the selection of electron-withdrawing group, halides, solvent mixture, and operating conditions, thereby broadening the range of applications for redox-mediated electrosorption in nonaqueous media.

## 3. CONCLUSIONS

We demonstrated selective XB electrosorption in nonaqueous media by designing a redox-active halogen bonding (XB) polymer P(FcTS-I). Upon electrochemical oxidation of ferrocene, a strong partial positive charge ($\sigma$-hole) was amplified, leading to enhanced electrosorption of various halides, oxyanions, and charged organic molecules. A 4.2-fold and up to 49-fold increase in the electrosorption for chloride and phenyl phosphonate was achieved, respectively, compared to the open-circuit potential. In addition, the halogen bonding platform was selective toward halides, exhibiting 1.3-fold and 2.4-fold enhanced chloride uptake, as well as 1.5-fold and 1.9-fold enhanced fluoride uptake, compared to P(FcTS) and PVF, due to its directional binding and affinity toward more electronegative ions. Moreover, thermodynamic selectivity analysis across halides and oxyanions validated the electrosorption results, highlighting the robust interaction between P(FcTS-I) and halides in comparison to that towards P(FcTS) or PVF. XB can be switched off upon reduction of ferrocene, resulting in the complete release of the bound chloride. NMR titration and Raman spectroscopy elucidated that XB serves as a primary selective interaction, with the ferrocene serving as a switch for controlling the strength of XB. DFT calculations provided evidence of the amplification of the $\sigma$-hole upon oxidation of ferrocene, and the importance of directional bindings for the strong charge transfer interactions between the $\sigma$-hole and target species. Based on the remarkable uptake of model organic species, such as benzenesulfonate and phenyl phosphonate, we can envision the capability of XB for ion-selective separations of a wide range of charge species beyond small ions. For a more comprehensive understanding of binding interactions, we acknowledge the potential importance of investigating molecular dynamics in future studies. Moving forward, the development of cascade electrosorption processes, as well as continuous flow systems, will further enhance the overall selective separation processes of P(FcTS-I), which are essential for practical industrial applications. Overall, our work demonstrated the electrochemically responsive XB donor polymer for selective electrosorption, holding great promise as a platform for electrochemical separation in organic media.

## 4. EXPERIMENTAL SECTION/METHODS

### 4.1. Materials

All chemicals were obtained from Sigma-Aldrich, TCI, VWR, AbaChemScene, and Fisher Scientific and used as received. Poly(vinyl ferrocene) was purchased from Polysciences, while FcTS-I, FcTS, and their polymers were prepared as described in SI 2.1, while the synthesis of 4-iodomorpholine-hydrogen iodide was referred to in the previous paper.[74] The detailed instrumentation for characterizing synthesized materials and the spectroscopic methods can be found in the Supporting Information (SI 1).

### 4.2. Electrode Synthesis and Characterization

The electrode was synthesized via the drop-casting method.[10,54,75] Redox-active polymers such as P(FcTS-I), P(FcTS), and PVF were dispersed with CNTs as a conducting additive with 1:0.5 mass ratios (8 mg:4 mg) in 2 mL of chloroform. The addition of CNTs does not contribute to electrosorption, as tested in chloride uptake with only CNT-coated carbon paper. Besides, the negligible capacitance was observed in the CV plot of the CNT-control electrode, suggesting that the uptake is likely originating from the polymers (Figure S2.23). As our experiment is conducted in an organic solvent, there is a possibility of metallopolymer electrodes leaching into the solution in the absence of a cross-linker, as demonstrated by the control CV experiment (Figure S2.24). To prevent this, we added 1,3-benzenedisulfonyl azide (15 wt % of metallopolymer) as a cross-linker to the mixture solution, prepared according to a previous paper.[76] When the temperature is increased above 120 °C, reactive nitrene species from 1,3-benzenedisulfonyl azide are formed, which insert into the C−H bonds of the polymer.[77] 50 $\mu$L of the electrode solution was drop-casted twice on the carbon paper electrode (1 cm × 1 cm). The coated electrode was dried in the oven at 140 °C for 2 h. According to the TGA, all three metallopolymers exhibit excellent thermal stability, especially at temperatures lower than 210 °C (Figure S2.18). Therefore, crosslinking the electrodes at 140 °C is unlikely to result in any degradation of the polymer. With the active surface of 1 cm × 1 cm, 100 $\mu$L drop-casting led to the final loading of 0.6 mg of redox-active material.

To observe electrode surface morphology, SEM (Axia ChemiSEM, Thermo Fisher) and energy-dispersive X-ray spectroscopy (EDS) were performed under high-vacuum Everhart−Thornley SE detector (ETD) mode with an accelerating voltage of 30 kV and a spot size of 4.0. Furthermore, the surface chemical compositions of heterogeneous electrodes (metallopolymer with CNT) were analyzed by X-ray photoelectron spectroscopy (XPS, MSE Supplies LLC) to evaluate the binding energies of C, N, O, Fe, and I (Figure S2.19). The XPS analysis revealed distinctive peaks of I 3d$_{3/2}$ and I 3d$_{5/2}$, corresponding to the iodide present in the P(FcTS-I) electrode. Additionally, there was a prominent N 1s peak indicating the presence of nitrogen atoms in the triazole group of both P(FcTS-I) and P(FcTS) electrodes.

### 4.3. Electrochemical Studies

Molecular recognition studies were conducted via a CV. The sensing capability of the redox-active polymer was measured by the peak shift of CV ($\Delta E_{1/2}$) in the absence and presence of the 10 mM of target species. All of the sensing experiments were conducted in 5 mL of solution with 100 mM TBAPF$_6$ as an electrolyte and the three-electrode system with Ag/AgNO$_3$ as a reference electrode. CV was run in 100 mM TBAPF$_6$ for 10 cycles under nitrogen to obtain the stable $E_{1/2}$ without the target species. Then, the solution was switched to 10 mM target anions along with 100 mM TBAPF$_6$ to run CV in the presence of the target species. $E_{1/2}$ was calculated with the third cycle and the difference in half-cell potential was compared among various target anions, including halides (F$^-$, Cl$^-$, Br$^-$, and I$^-$) and oxyanions (H$_2$PO$_4^-$, HSO$_4^-$, NO$_3^-$, ReO$_4^-$ and ClO$_4^-$). The Biologic software was used to calculate the peak current and corresponding potentials in order to determine $E_{1/2}$ and $\Delta E_{1/2}$. However, due to the broad peak shape observed when strong binding target species (e.g., Cl$^-$) were introduced, there was a chance of encountering errors. To address the potential errors resulting from peak selection, we conducted anion recognition experiments twice with fresh solutions and newly synthesized electrodes. The error bars for $\Delta E_{1/2}$

demonstrated that the error caused by broad peaks was minimal, with an average standard deviation of $\pm 1.7$ mV. This minimal error did not significantly affect the trend in binding strength among the various anions.

The electrosorption test was conducted in chronoamperometry mode for 15 min in the three-electrode system with $Ag/AgNO_3$ as a reference electrode. With linear sweep voltammetry, we selected an adsorption potential of 0.3 V with respect to $E_{1/2}$ for all adsorption tests to avoid side reactions and provide equivalent redox reactions among the three metallopolymers (Figure S3.2). For the electrosorption test, we adjusted the ionic strength for the electrosorption to enhance the accuracy of the measurements. To verify the concentration difference ($\Delta C$ = approximately 0.1 mM) before and after the electrosorption tests, we used 10 times lower ion concentrations (1 mM TBACl in 10 mM TBAPF$_6$) than those used in the anion recognition tests (10 mM TBACl in 100 mM TBAPF$_6$). Unless specified otherwise, the adsorption test consisted of 5 mL of a solution containing 1 mM target species and 10 mM TBAPF$_6$, while the desorption test used 20 mM TBABF$_4$ under nitrogen. We conducted three identical adsorption experiments with fresh solutions and newly synthesized electrodes to demonstrate the reproducibility of our results.

The concentrations of target species were measured by ion chromatography (IC, Dionex Integration, Thermo Fisher Scientific) for small anions such as $F^-$, $Cl^-$, $H_2PO_4^-$, $HSO_4^-$, $NO_3^-$, and $PF_6^-$. Since our experiments were conducted in organic solvents with hexafluorophosphate ($PF_6^-$) or tetrafluoroborate ($BF_4^-$) with an IonPac AS-22 column, the mixture of DI and acetonitrile was used as an eluent solvent.[78] The fresh eluent was prepared with 4.5 mM NaHCO$_3$ and 1.4 mM Na$_2$CO$_3$ of a mixture of DI and acetonitrile with 70 vol %:30 vol % and preserved under nitrogen. The samples were run at a flow rate of 0.9 mL/min for 18 min to detect $F^-$, $Cl^-$, $H_2PO_4^-$, $HSO_4^-$, $NO_3^-$, and $PF_6^-$. Plasma-optical emission spectrometry (5110 ICP-OES, Agilent) was used for measuring the uptake of $ReO_4^-$ with an eluent solution of 5 wt % nitric acid. Moreover, high-performance liquid chromatography (HPLC, Agilent 1260 Infinity II, Agilent) was used for charged organic species such as benzenesulfonate and phenyl phosphonate. The organic acid concentration was measured by HPLC with the C$_{18}$ column (4.6 mm × 100 mm × 2.7 $\mu$m, Agilent Poroshell 120) at the flow rate of 0.5 mL/min. 5% of phase A (Acetonitrile) and 95% of phase B (0.1% trifluoroacetic acid (TFA) in DI) were used with the sample injection volume of 5 $\mu$L for 8 min.

### 4.4. Computational Methods

Avogadro 1.2.0[79] was used for generating initial coordinates for all structures (target species and redox complexes), while DFT calculations were calculated using ORCA 5.0.2. Geometry optimizations and Hessian calculations were carried out at the $\omega$B97X-D3(BJ)/[80]ma-def2-TZVP/[81]SMD[82] level of theory with the def2-ECP pseudopotential[83] for metals as implemented in ORCA 5.0.2 software.[84] The RIJCOSX method[85] along with the auxiliary def2-TZVP basis set was used to accelerate hybrid DFT calculations. BSSE errors were not computed, as the large basis sets were employed in calculations. Default ORCA values for force and energy tolerances were used. We have chosen the SMD solvation model over the CPCM model due to the least deviation of calculated solvation-free energies of monatomic anions (chloride) from previous computational results. In particular, we found the solvation-free energy of $Cl^-$ in $CH_3CN$ computed with SMD ($-66.02$ kcal/mol) at 298 K and 1 atm to be closer to the value obtained by Kelly et al.[86] using cluster pair approximation ($-60.5$ kcal/mol), compared to CPCM ($-71.71$ kcal/mol). The default SMD parameters, as implemented in ORCA 5.0.2, were used. The comprehensive methodology for the computational work is provided in the Supporting Information (SI 1).

### ■ ASSOCIATED CONTENT

#### ⓢ Supporting Information

The Supporting Information is available free of charge at https://pubs.acs.org/doi/10.1021/jacsau.4c00265.

Experimental methods, synthesis information and material characterization (mass spectrum, GPC, and 2D NMR), CV peak shift, NMR titrations, bonding interaction motion corresponding to Raman shift, and the possible binding orientations (PDF)

### ■ AUTHOR INFORMATION

#### Corresponding Author

**Xiao Su** − *Department of Chemical and Biomolecular Engineering, University of Illinois Urbana−Champaign, Urbana, Illinois 61801, United States;* ⓘ orcid.org/0000-0001-7794-290X; Email: x2su@illinois.edu

#### Authors

**Nayeong Kim** − *Department of Chemical and Biomolecular Engineering, University of Illinois Urbana−Champaign, Urbana, Illinois 61801, United States;* ⓘ orcid.org/0000-0002-5452-1085

**Vijaya S. Jeyaraj** − *Department of Chemical and Biomolecular Engineering, University of Illinois Urbana−Champaign, Urbana, Illinois 61801, United States;* ⓘ orcid.org/0000-0003-2109-4299

**Johannes Elbert** − *Department of Chemical and Biomolecular Engineering, University of Illinois Urbana−Champaign, Urbana, Illinois 61801, United States;* ⓘ orcid.org/0000-0002-7682-8686

**Sung Jin Seo** − *Department of Chemical and Biomolecular Engineering, University of Illinois Urbana−Champaign, Urbana, Illinois 61801, United States*

**Alexander V. Mironenko** − *Department of Chemical and Biomolecular Engineering, University of Illinois Urbana−Champaign, Urbana, Illinois 61801, United States;* ⓘ orcid.org/0000-0001-7490-5038

Complete contact information is available at:
https://pubs.acs.org/10.1021/jacsau.4c00265

#### Author Contributions

N.K.: conceptualization, material synthesis, methodology, validation, investigation, writing and editing of the original draft, visualization. V.S.J.: investigation, validation, reviewing and editing of the original draft. J.E.: conceptualization, material synthesis, reviewing and editing of the original draft. S.J.S.: investigation. A.V.M.: validation, reviewing and editing of the original draft. X.S.: conceptualization, reviewing and editing the original draft, supervision, and funding acquisition. CRediT: **Nayeong Kim** conceptualization, data curation, formal analysis, investigation, methodology, writing-original draft, writing-review & editing; **Vijaya Sundar Jeyaraj** investigation, methodology, software, writing-review & editing; **Johannes Elbert** conceptualization, investigation, methodology, writing-review & editing; **Sung Jin Seo** investigation, methodology; **Alexander V. Mironenko** investigation, methodology, resources, software, supervision, writing-review & editing; **Xiao Su** conceptualization, investigation, project administration, writing-original draft, writing-review & editing.

#### Notes

The authors declare no competing financial interest.

## ACKNOWLEDGMENTS

## REFERENCES

(1) Yang, X.; Liu, T.; Li, R.; Yang, X.; Lyu, M.; Fang, L.; Zhang, L.; Wang, K.; Zhu, A.; Zhang, L.; Qiu, C.; Zhang, Y.-Z.; Wang, X.; Peng, L.-M.; Yang, F.; Li, Y. Host–guest molecular interaction enabled separation of large-diameter semiconducting single-walled carbon nanotubes. *J. Am. Chem. Soc.* **2021**, *143* (27), 10120–10130.

(2) Xie, Y.; Cui, H.; Wu, H.; Lin, R. B.; Zhou, W.; Chen, B. Electrostatically driven selective adsorption of carbon dioxide over acetylene in an ultramicroporous material. *Angew. Chem., Int. Ed.* **2021**, *133* (17), 9690–9695.

(3) Chen, C.; Guan, H.; Li, H.; Zhou, Y.; Huang, Y.; Wei, W.; Hong, M.; Wu, M. A Noncovalent π-Stacked Porous Organic Molecular Framework for Selective Separation of Aromatics and Cyclic Aliphatics. *Angew. Chem., Int. Ed.* **2022**, *61*, No. e202201646.

(4) Su, X. Electrochemical interfaces for chemical and biomolecular separations. *Current opinion in colloid & interface science* **2020**, *46*, 77–93.

(5) Alkhadra, M. A.; Su, X.; Suss, M. E.; Tian, H.; Guyes, E. N.; Shocron, A. N.; Conforti, K. M.; de Souza, J. P.; Kim, N.; Tedesco, M.; Khoiruddin, K.; Wenten, I. G.; Santiago, J. G.; Hatton, T. A.; Bazant, M. Z. Electrochemical methods for water purification, ion separations, and energy conversion. *Chem. Rev.* **2022**, *122* (16), 13547–13635.

(6) Clarke, C. J.; Tu, W.-C.; Levers, O.; Brohl, A.; Hallett, J. P. Green and sustainable solvents in chemical processes. *Chem. Rev.* **2018**, *118* (2), 747–800.

(7) Shi, X.; Zhang, Z.; Yin, C.; Zhang, X.; Long, J.; Zhang, Z.; Wang, Y. Design of Three-Dimensional Covalent Organic Framework Membranes for Fast and Robust Organic Solvent Nanofiltration. *Angew. Chem.* **2022**, *61* (36), No. e202207559.

(8) Constable, D. J.; Jimenez-Gonzalez, C.; Henderson, R. K. Perspective on solvent use in the pharmaceutical industry. *Organic process research & development* **2007**, *11* (1), 133–137.

(9) Kim, K.; Raymond, D.; Candeago, R.; Su, X. Selective cobalt and nickel electrodeposition for lithium-ion battery recycling through integrated electrolyte and interface control. *Nat. Commun.* **2021**, *12* (1), 6554.

(10) Chen, R.; Feng, J.; Jeon, J.; Sheehan, T.; Rüttiger, C.; Gallei, M.; Shukla, D.; Su, X. Structure and Potential-Dependent Selectivity in Redox-Metallopolymers: Electrochemically Mediated Multicomponent Metal Separations. *Adv. Funct. Mater.* **2021**, *31* (15), 2009307.

(11) Kim, N.; Oh, W.; Knust, K. N.; Zazyki Galetto, F.; Su, X. Molecularly Selective Polymer Interfaces for Electrochemical Separations. *Langmuir* **2023**, *47*, 16685.

(12) Srimuk, P.; Su, X.; Yoon, J.; Aurbach, D.; Presser, V. Charge-transfer materials for electrochemical water desalination, ion separation and the recovery of elements. *Nature Reviews Materials* **2020**, *5* (7), 517–538.

(13) Gamaethiralalage, J.; Singh, K.; Sahin, S.; Yoon, J.; Elimelech, M.; Suss, M.; Liang, P.; Biesheuvel, P.; Zornitta, R. L.; De Smet, L. Recent advances in ion selectivity with capacitive deionization. *Energy Environ. Sci.* **2021**, *14* (3), 1095–1120.

(14) Cotty, S.; Jeon, J.; Elbert, J.; Jeyaraj, V. S.; Mironenko, A. V.; Su, X. Electrochemical recycling of homogeneous catalysts. *Sci. Adv.* **2022**, *8* (42), No. eade3094.

(15) Román Santiago, A.; Yin, S.; Elbert, J.; Lee, J.; Shukla, D.; Su, X. Imparting Selective Fluorophilic Interactions in Redox Copolymers for the Electrochemically Mediated Capture of Short-Chain Perfluoroalkyl Substances. *J. Am. Chem. Soc.* **2023**, *145* (17), 9508–9519.

(16) Cotty, S. R.; Kim, N.; Su, X. Electrochemically Mediated Recovery and Purification of Gold for Sustainable Mining and Electronic Waste Recycling. *ACS Sustainable Chem. Eng.* **2023**, *11* (9), 3975–3986.

(17) Kim, N.; Lee, J.; Su, X. Precision Tuning of Highly Selective Polyelectrolyte Membranes for Redox-Mediated Electrochemical Separation of Organic Acids. *Adv. Funct. Mater.* **2023**, *33* (12), 2211645.

(18) Kim, N.; Jeon, J.; Chen, R.; Su, X. Electrochemical separation of organic acids and proteins for food and biomanufacturing. *Chem. Eng. Res. Des.* **2022**, *178*, 267–288.

(19) Cavallo, G.; Metrangolo, P.; Milani, R.; Pilati, T.; Priimagi, A.; Resnati, G.; Terraneo, G. The halogen bond. *Chem. Rev.* **2016**, *116* (4), 2478–2601.

(20) Metrangolo, P.; Meyer, F.; Pilati, T.; Resnati, G.; Terraneo, G. Halogen bonding in supramolecular chemistry. *Angew. Chem., Int. Ed.* **2008**, *47* (33), 6114–6127.

(21) Evans, N. H.; Beer, P. D. Advances in anion supramolecular chemistry: from recognition to chemical applications. *Angew. Chem., Int. Ed.* **2014**, *53* (44), 11716–11754.

(22) Gilday, L. C.; Robinson, S. W.; Barendt, T. A.; Langton, M. J.; Mullaney, B. R.; Beer, P. D. Halogen bonding in supramolecular chemistry. *Chem. Rev.* **2015**, *115* (15), 7118–7195.

(23) Auffinger, P.; Hays, F. A.; Westhof, E.; Ho, P. S. Halogen bonds in biological molecules. *Proc. Natl. Acad. Sci. U. S. A.* **2004**, *101* (48), 16789–16794.

(24) Abe, A.; Goushi, K.; Mamada, M.; Adachi, C. Organic Binary and Ternary Cocrystal Engineering Based on Halogen Bonding Aimed at Room-Temperature Phosphorescence. *Adv. Mater.* **2023**, *36*, 2211160.

(25) Fave, C.; Schöllhorn, B. Electrochemical activation of halogen bonding. *Current Opinion in Electrochemistry* **2019**, *15*, 89–96.

(26) Oliveira, R.; Groni, S.; Fave, C.; Branca, M.; Mavré, F.; Lorcy, D.; Fourmigué, M.; Schöllhorn, B. Electrochemical activation of a tetrathiafulvalene halogen bond donor in solution. *Phys. Chem. Chem. Phys.* **2016**, *18* (23), 15867–15873.

(27) Lim, J. Y.; Beer, P. D. A halogen bonding 1, 3-disubstituted ferrocene receptor for recognition and redox sensing of azide. *Eur. J. Inorg. Chem.* **2017**, *2017* (2), 220–224.

(28) Mondal, S.; Giri, D.; Mugesh, G. Halogen Bonding in the Molecular Recognition of Thyroid Hormones and Their Metabolites by Transport Proteins and Thyroid Hormone Receptors. *Journal of the Indian Institute of Science* **2020**, *100* (1), 231–247.

(29) Kilah, N. L.; Wise, M. D.; Serpell, C. J.; Thompson, A. L.; White, N. G.; Christensen, K. E.; Beer, P. D. Enhancement of anion recognition exhibited by a halogen-bonding rotaxane host system. *J. Am. Chem. Soc.* **2010**, *132* (34), 11893–11895.

(30) Liu, Q.; Zhao, C.; Shao, X.; Wang, W.; Ji, X. High sensitive pyridine chemiresistive sensors based on azacyclobutane modified perylene bisimide derivatives. *Dyes Pigm.* **2021**, *185*, No. 108902.

(31) Jaini, A. K.; Hughes, L. B.; Kitimet, M. M.; Ulep, K. J.; Leopold, M. C.; Parish, C. A. Halogen bonding interactions for aromatic and nonaromatic explosive detection. *ACS sensors* **2019**, *4* (2), 389–397.

(32) Bulfield, D.; Huber, S. M. Halogen bonding in organic synthesis and organocatalysis. *Chem. - Eur. J.* **2016**, *22* (41), 14434–14450.

(33) Sutar, R. L.; Huber, S. M. Catalysis of organic reactions through halogen bonding. *ACS Catal.* **2019**, *9* (10), 9622–9639.

(34) Aubert, E.; Doudouh, A.; Wenger, E.; Sechi, B.; Peluso, P.; Pale, P.; Mamane, V. Chiral Ferrocenyl– Iodotriazoles and– Iodotriazoliums as Halogen Bond Donors. Synthesis, Solid State Analysis and Catalytic Properties. *Eur. J. Inorg. Chem.* **2022**, *2022* (5), No. e202100927.

(35) Pancholi, J.; Beer, P. D. Halogen bonding motifs for anion recognition. *Coord. Chem. Rev.* **2020**, *416*, No. 213281.

(36) Parker, A. J.; Stewart, J.; Donald, K. J.; Parish, C. A. Halogen bonding in DNA base pairs. *J. Am. Chem. Soc.* **2012**, *134* (11), 5165–5172.

(37) Lu, Y.; Wang, Y.; Zhu, W. Nonbonding interactions of organic halogens in biological systems: implications for drug discovery and

biomolecular design. *Phys. Chem. Chem. Phys.* **2010**, *12* (18), 4543−4551.

(38) Patrick, S. C.; Hein, R.; Beer, P. D.; Davis, J. J. Continuous and Polarization-Tuned Redox Capacitive Anion Sensing at Electroactive Interfaces. *J. Am. Chem. Soc.* **2021**, *143* (45), 19199−19206.

(39) Priimagi, A.; Saccone, M.; Cavallo, G.; Shishido, A.; Pilati, T.; Metrangolo, P.; Resnati, G. Photoalignment and Surface-Relief-Grating Formation are Efficiently Combined in Low-Molecular-Weight Halogen-Bonded Complexes. *Adv. Mater.* **2012**, *24* (44), OP345−OP352.

(40) Jentzsch, A. V.; Matile, S.Anion transport with halogen bonds. *Halogen Bonding I: Impact on Materials Chemistry and Life Sciences***2015**, 205−239.

(41) Kampes, R.; Zechel, S.; Hager, M. D.; Schubert, U. S. Halogen bonding in polymer science: towards new smart materials. *Chemical Science* **2021**, *12* (27), 9275−9286.

(42) Priimagi, A.; Cavallo, G.; Metrangolo, P.; Resnati, G. The halogen bond in the design of functional supramolecular materials: recent advances. *Accounts of chemical research* **2013**, *46* (11), 2686−2695.

(43) Biswas, S.; Das, A. Recent Developments in Polymeric Assemblies and Functional Materials by Halogen Bonding. *ChemNanoMat* **2021**, *7* (7), 748−772.

(44) Bertani, R.; Metrangolo, P.; Moiana, A.; Perez, E.; Pilati, T.; Resnati, G.; Rico-Lattes, I.; Sassi, A. Supramolecular Route to Fluorinated Coatings: Self-Assembly Between Poly (4-vinylpyridines) and Haloperfluorocarbons. *Adv. Mater.* **2002**, *14* (17), 1197−1201.

(45) Lim, J. Y.; Cunningham, M. J.; Davis, J. J.; Beer, P. D. Halogen bonding-enhanced electrochemical halide anion sensing by redox-active ferrocene receptors. *Chem. Commun.* **2015**, *51* (78), 14640−14643.

(46) Tepper, R.; Bode, S.; Geitner, R.; Jäger, M.; Görls, H.; Vitz, J.; Dietzek, B.; Schmitt, M.; Popp, J.; Hager, M. D.; Schubert, U. S. Polymeric Halogen-Bond-Based Donor Systems Showing Self-Healing Behavior in Thin Films. *Angew. Chem., Int. Ed.* **2017**, *56* (14), 4047−4051.

(47) Pang, P.; Miao, X.; Ying, L.; Kong, G.; Che, C.; Deng, W. Halogen-bond-controlled self-assembly of Regioisomeric Phenanthridine derivatives into nanowires and Nanosheets. *J. Phys. Chem. C* **2020**, *124* (10), 5665−5671.

(48) Hein, R.; Borissov, A.; Smith, M. D.; Beer, P. D.; Davis, J. J. A halogen-bonding foldamer molecular film for selective reagentless anion sensing in water. *Chem. Commun.* **2019**, *55* (33), 4849−4852.

(49) Hein, R.; Li, X.; Beer, P. D.; Davis, J. J. Enhanced voltammetric anion sensing at halogen and hydrogen bonding ferrocenyl SAMs. *Chemical Science* **2021**, *12* (7), 2433−2440.

(50) Hijazi, H.; Vacher, A.; Groni, S.; Lorcy, D.; Levillain, E.; Fave, C.; Schöllhorn, B. Electrochemically driven interfacial halogen bonding on self-assembled monolayers for anion detection. *Chem. Commun.* **2019**, *55* (13), 1983−1986.

(51) Patrick, S. C.; Hein, R.; Docker, A.; Beer, P. D.; Davis, J. J. Solvent Effects in Halogen and Hydrogen Bonding Mediated Electrochemical Anion Sensing in Aqueous Solution and at Interfaces. *Chem. - Eur. J.* **2021**, *27* (39), 10201−10209.

(52) Kim, N.; Elbert, J.; Kim, C.; Su, X. Redox-copolymers for nanofiltration-enabled electrodialysis. *ACS Energy Letters* **2023**, *8* (5), 2097−2105.

(53) Glaser, R.; Chen, N.; Wu, H.; Knotts, N.; Kaupp, M. 13C NMR study of halogen bonding of haloarenes: measurements of solvent effects and theoretical analysis. *J. Am. Chem. Soc.* **2004**, *126* (13), 4412−4419.

(54) Su, X.; Kulik, H. J.; Jamison, T. F.; Hatton, T. A. Anion-selective redox electrodes: electrochemically mediated separation with heterogeneous organometallic interfaces. *Adv. Funct. Mater.* **2016**, *26* (20), 3394−3404.

(55) Su, X.; Kushima, A.; Halliday, C.; Zhou, J.; Li, J.; Hatton, T. A. Electrochemically-mediated selective capture of heavy metal chromium and arsenic oxyanions from water. *Nat. Commun.* **2018**, *9* (1), 4701.

(56) Costentin, C.; Saveant, J.-M. Cyclic voltammetry analysis of electrocatalytic films. *J. Phys. Chem. C* **2015**, *119* (22), 12174−12182.

(57) Zapata, F.; Caballero, A.; Molina, P. Ferrocene−Triazole Combination as a Benchmark for the Electrochemical Detection of Noncovalent Halogen-Bonding Interactions. *Eur. J. Inorg. Chem.* **2017**, *2017* (2), 237−241.

(58) Hein, R.; Beer, P. D. Halogen bonding and chalcogen bonding mediated sensing. *Chemical Science* **2022**, *13* (24), 7098−7125.

(59) Erdelyi, M. Halogen bonding in solution. *Chem. Soc. Rev.* **2012**, *41* (9), 3547−3557.

(60) Lim, J. Y.; Marques, I.; Ferreira, L.; Félix, V.; Beer, P. D. Enhancing the enantioselective recognition and sensing of chiral anions by halogen bonding. *Chem. Commun.* **2016**, *52* (32), 5527−5530.

(61) Giron, R. G. P.; Ferguson, G. S. Tetrafluoroborate and hexafluorophosphate ions are not interchangeable: a density functional theory comparison of hydrogen bonding. *ChemistrySelect* **2017**, *2* (33), 10895−10901.

(62) Duarte, D. J.; Angelina, E. L.; Peruchena, N. M. On the strength of the halogen bonds: mutual penetration, atomic quadrupole moment and Laplacian distribution of the charge density analyses. *Computational and Theoretical Chemistry* **2012**, *998*, 164−172.

(63) Ouvrard, C.; Berthelot, M.; Laurence, C. The first basicity scale of fluoro-, chloro-, bromo- and iodo-alkanes: some cross-comparisons with simple alkyl derivatives of other elements. *J. Chem. Soc.* **1999**, *7*, 1357−1362. Perkin Transactions 2

(64) Bard, A. J.; Faulkner, L. R.; White, H. S.*Electrochemical methods: fundamentals and applications*; John Wiley & Sons, 2022.

(65) Gale, P. A.; Hursthouse, M. B.; Light, M. E.; Sessler, J. L.; Warriner, C. N.; Zimmerman, R. S. Ferrocene-substituted calix [4] pyrrole: a new electrochemical sensor for anions involving CH··· anion hydrogen bonds. *Tetrahedron Lett.* **2001**, *42* (38), 6759−6762.

(66) Bluemel, J.; Hebendanz, N.; Hudeczek, P.; Koehler, F. H.; Strauss, W. Synthesis and NMR spectroscopy of metallocenium ions. Support for a new ferromagnetic coupling mechanism in decamethyl-metallocenium tetracyanoethenides. *J. Am. Chem. Soc.* **1992**, *114* (11), 4223−4230.

(67) Vícha, J.; Novotny, J.; Komorovsky, S.; Straka, M.; Kaupp, M.; Marek, R. Relativistic heavy-neighbor-atom effects on NMR shifts: Concepts and trends across the periodic table. *Chem. Rev.* **2020**, *120* (15), 7065−7103.

(68) Sarwar, M. G.; Dragisic, B.; Salsberg, L. J.; Gouliaras, C.; Taylor, M. S. Thermodynamics of halogen bonding in solution: substituent, structural, and solvent effects. *J. Am. Chem. Soc.* **2010**, *132* (5), 1646−1653.

(69) Vidiakina, A.; Bogachev, N.; Skripkin, M. Y.; Mereshchenko, A. Study of Tetraethylammonium and Lithium Chlorides Dissociation in Acetonitrile Solutions. *Russian Journal of General Chemistry* **2020**, *90*, 1703−1705.

(70) Tsona, N. T.; Henschel, H.; Bork, N.; Loukonen, V.; Vehkamaki, H. Structures, hydration, and electrical mobilities of bisulfate ion−sulfuric acid−ammonia/dimethylamine clusters: a computational study. *J. Phys. Chem. A* **2015**, *119* (37), 9670−9679.

(71) Ge, L.; Bernasconi, L.; Hunt, P. Linking electronic and molecular structure: insight into aqueous chloride solvation. *Phys. Chem. Chem. Phys.* **2013**, *15* (31), 13169−13183.

(72) Sato, K.; Hyodo, M.; Aoki, M.; Zheng, X.-Q.; Noyori, R. Oxidation of sulfides to sulfoxides and sulfones with 30% hydrogen peroxide under organic solvent-and halogen-free conditions. *Tetrahedron* **2001**, *57* (13), 2469−2476.

(73) Ananchenko, G.; Novakovic, J.; Lewis, J. Amlodipine besylate. *Profiles of Drug Substances, Excipients and Related Methodology* **2012**, *37*, 31−77.

(74) Spiteri, C.; Moses, J. E. Copper-catalyzed azide−alkyne cycloaddition: regioselective synthesis of 1, 4, 5-trisubstituted 1, 2, 3-triazoles. *Angew. Chem., Int. Ed.* **2010**, *49* (1), 31−33.

(75) Kim, K.; Cotty, S.; Elbert, J.; Chen, R.; Hou, C.; S-H.u, X. Asymmetric redox-polymer interfaces for electrochemical reactive separations: synergistic capture and conversion of arsenic. *Adv. Mater.* **2020**, *32* (6), 1906877.

(76) Baker, D.; East, G.; Mukhopadhyay, S. Synthesis and characterization of some disulfonyl azides as potential crosslinking agents for textile fibers. *J. Appl. Polym. Sci.* **2001**, *79* (6), 1092−1100.

(77) Pandiyarajan, C.; Rubinstein, M.; Genzer, J. Surface-anchored poly (N-isopropylacrylamide) orthogonal gradient networks. *Macromolecules* **2016**, *49* (14), 5076−5083.

(78) Terborg, L.; Nowak, S.; Passerini, S.; Winter, M.; Karst, U.; Haddad, P. R.; Nesterenko, P. N. Ion chromatographic determination of hydrolysis products of hexafluorophosphate salts in aqueous solution. *Analytica chimica acta* **2012**, *714*, 121−126.

(79) Hanwell, M. D.; Curtis, D. E.; Lonie, D. C.; Vandermeersch, T.; Zurek, E.; Hutchison, G. R. Avogadro: An advanced semantic chemical editor, visualization, and analysis platform. *J. Cheminf.* **1758**, *4* (17), 17.

(80) Najibi, A.; Goerigk, L. The nonlocal kernel in van der Waals density functionals as an additive correction: An extensive analysis with special emphasis on the B97M-V and ωB97M-V approaches. *J. Chem. Theory Comput.* **2018**, *14* (11), 5725−5738.

(81) Zheng, J.; Xu, X.; Truhlar, D. G. Minimally augmented Karlsruhe basis sets. *Theor. Chem. Acc.* **2011**, *128* (3), 295−305.

(82) Grisafi, A.; Wilkins, D. M.; Csányi, G.; Ceriotti, M. Symmetry-adapted machine learning for tensorial properties of atomistic systems. *Physical review letters* **2018**, *120* (3), No. 036002.

(83) Weigend, F.; Ahlrichs, R. Balanced basis sets of split valence, triple zeta valence and quadruple zeta valence quality for H to Rn: Design and assessment of accuracy. *Phys. Chem. Chem. Phys.* **2005**, *7* (18), 3297−3305.

(84) Neese, F.; Wennmohs, F.; Becker, U.; Riplinger, C. The ORCA quantum chemistry program package. *J. Chem. Phys.* **2020**, *152* (22), 224108.

(85) Neese, F.; Wennmohs, F.; Hansen, A.; Becker, U. Efficient, approximate and parallel Hartree−Fock and hybrid DFT calculations. A 'chain-of-spheres' algorithm for the Hartree−Fock exchange. *Chem. Phys.* **2009**, *356* (1−3), 98−109.

(86) Kelly, C. P.; Cramer, C. J.; Truhlar, D. G. Single-ion solvation free energies and the normal hydrogen electrode potential in methanol, acetonitrile, and dimethyl sulfoxide. *J. Phys. Chem. B* **2007**, *111* (2), 408−422.